JPL Publication 87-10

Optimum Filters and Smoothers Design for Carrier Phase and Frequency Tracking

R. Kumar

May 1, 1987

National Aeronautics and Space Administration

Jet Propulsion Laboratory
California Institute of Technology
Pasadena, California

JPL Publication 87-10

Optimum Filters and Smoothers Design for Carrier Phase and Frequency Tracking

R. Kumar

May 1, 1987

National Aeronautics and
Space Administration

Jet Propulsion Laboratory
California Institute of Technology
Pasadena, California

The research described in this publication was carried out by the Jet Propulsion Laboratory, California Institute of Technology, and sponsored by California State University, Long Beach, and by the National Aeronautics and Space Administration.

Preface

While the work described in this report was performed by the author at the Jet Propulsion Laboratory, he is also an Associate Professor of Electrical Engineering at California State University, Long Beach, California.

Abstract

The report presents the application of fixed lag smoothing algorithms to the problem of estimation of the phase and frequency of a sinusoidal carrier received in the presence of process noise and additive observation noise. A suboptimal structure consists of a phase-locked loop (PLL) followed by a post-loop correction to the phase and frequency estimates. When the PLL is operating under high signal-to-noise ratio, the phase detector is approximately linear, and the smoother equations then correspond to the optimal linear equations for an equivalent linear signal model. The performance of such a smoother can be predicted by linear filtering theory. However, if the PLL is operating near the threshold region of the signal-to-noise ratio, the phase detector cannot be assumed to be linear. Then the actual performance of the smoother can significantly differ from that predicted by linear theory. In this report we present both the theoretical and simulated performance of such smoothers derived on the basis of various models for the phase and frequency processes.

Contents

Figures

I. Introduction

The derivation of optimum receivers through modern estimation techniques has been proposed by various researchers [1-12] (see also their references). In references [4,5] optimum zero lag receivers have been derived on the basis of linear Kalman filtering theory [6] for linear measurement schemes. The nonlinear measurement situations which are of interest here have been studied in [7], wherein, on the basis of nonlinear filters of [8], suboptimal nonlinear zero lag receivers have been derived for the demodulation of angle modulated signals. In [9] the techniques of [7,8] have been extended to design suboptimum nonlinear fixed lag smoothers for phase estimation (see also [10-14]). The solution of the optimum nonlinear filtering and smoothing problem is, of course, intractable.

Whether derived from linear or nonlinear theory, the smoother structure consists of a phase-locked loop (PLL) followed by a post-loop correction to the phase and frequency estimates. In this report we study the application of linear and nonlinear smoothers to the estimation of phase and frequency of the sinusoid. We show that for this case, the suboptimum nonlinear smoother equations derived from [7,8,9] are not substantially different from the optimum linear smoother equations. In addition, simulations show that the difference in performance of the nonlinear and linear smoothers is small.

In this report we evaluate the performance of smoothers both by analysis and simulations. For high signal-to-noise ratio conditions when the phase detector can be assumed to be linear, the results predicted from linear theory are in close conformity with those obtained from simulations.

However, when the phase detector is highly nonlinear, the linear theory is inadequate to predict performance even for linear smoothers.

The performance of the smoother with a nonlinear phase detector is evaluated by simulations. When compared to the case of a linear phase detector the performance of the smoother can be substantially different. The difference can be much more pronounced when the process noise is present, compared to the case when only the observation noise is present. The simulation examples indicate that in the absence of process noise, although there is a significant performance degradation due to nonlinearity (about 1 dB when operating in the loop SNR of about 5 dB), there is no threshold observed in the smoothing error covariance in this region. In contrast to this, there is a pronounced threshold in the smoother performance when the process noise is present and the inverse of filter phase error variance is below 7.5 dB.

We also evaluate the smoother performance when the process noise is reduced in magnitude. That is, the smoother/filter solutions are based on a relatively high process noise, but in the simulation the actual variance of the process noise used is lower or zero. This is of interest because, in many practical applications, the process noise statistics are not precisely known, and are therefore deliberately overestimated.

In Section II we present the signal model and the suboptimum smoother equations as derived from the stochastic optimization theory. With a minor modification these equations are shown to be the linear Kalman filter equations for an appropriate linear signal model applicable when the phase detector can be assumed to be linear. This section also presents a simple finite impulse response (FIR) filter implementation of the smoother. Under

steady-state conditions, the coefficients of the FIR filter are constant and can be precomputed.

Section III presents three specific subcases of the signal model that are commonly used in the present application including those involving the phase and frequency estimation for communication and navigation systems. In this section, assuming the phase detector to be linear, closed-form expressions are derived for the filter and smoother transfer functions and their performance indices.

Section IV contains the simulation results for both linear and nonlinear phase detectors and compares the simulation results to those obtained from theory.

Finally, some concluding remarks are made in the last section. Detailed derivations are contained in Appendices A to C. Appendix D also contains the flow chart for the computer program developed for the above simulations and computations.

II. Signal Model and Smoother Equations

We consider the problem of estimating the phase process $\theta(k)$ from the sampled version of the received carrier signal $y(k)$, i.e.,

$$y(k) = A\sqrt{2}\ \mathrm{Sin}\ (\omega_c t_k + \theta(k)) + \bar{v}(k) \tag{1}$$

where t_k is the kth sampling time, ω_c is the known carrier frequency and $\bar{v}(k)$ the observation noise is the sampled version of a narrow band zero mean white Gaussian noise process $v(t)$. Furthermore, the phase process $\theta(k)$ is modeled as

$$\theta(k) = \beta \ell' x(k) \quad ; \quad \ell' = [10\ldots0]$$

$$x(k+1) = \Phi x(k) + w(k) \tag{2}$$

In (2), β is the phase constant, $x(k)$ is the state vector of dimension n, Φ is an (n x n) matrix and $w(k)$ is zero mean white Gaussian noise process independent of $\{\bar{v}(k)\}$. Thus

$$E[\bar{v}(k)] = 0 \quad , E[w(k)] = 0$$

$$E[\bar{v}^2(k)] = R \quad ; E[w(k)w^T(k)] = Q \quad ; E[\bar{v}(k)\ w(j)] = 0$$

Three possible values of n are considered in the sequel corresponding to first, second and third order smoothers. The specific selection of the matrices Q and Φ is considered later.

Applying the imbedding approach of [14], in reference [9], the suboptimal nonlinear equations have been derived from the nonlinear filter equations of [8]. These equations are presented in appendix A.

As shown in appendix A, when $2\omega_c t$ and higher order harmonic terms are ignored, the smoother equations reduce to the following

$$\begin{aligned}
\hat{x}_0(k+1) &= \Phi \hat{x}_0(k/k) + K_0(k+1)\eta(k+1) \\
\hat{x}_i(k+1/k+1) &= \hat{x}_{i-1}(k/k) + K_i(k+1)\eta(k+1) \\
\eta(k+1) &= \sqrt{2}\, y(k+1)\mathrm{Cos}(\hat{\theta}(k+1)) \\
\hat{\theta}(k+1) &= \omega_c t_{k+1} + \beta \ell' \hat{x}(k+1/k) \\
x_i(k) &\triangleq x(k-i) \quad ; \; i=0,\ldots L
\end{aligned} \tag{3}$$

In (3) $\hat{x}_i(k/j)$ denotes the estimate of $x_i(k)$ on the basis of observations up to time j and the gain vectors K_i and the cross covariance matrices $P_{i0}(k/j) \triangleq E\{\tilde{x}(k-i/j)\, \tilde{x}^T(k/j)\}$ are given by

$$K_i(k+1) = A\beta P_{i0}(k+1/k)\, \ell\, S^{-1}(k+1) \quad ; \quad 0 \le i \le L \tag{4}$$

$$P_{i0}(k+1/k+1) = P_{i0}(k+1/k) - P_{i0}(k+1/k)(A\beta\ell)(A\beta\ell)' P_{00}(k+1/k) S^{-1}(k+1) \tag{5a}$$

$$P_{i0}(k+1/k) = P_{i-1,0}(k/k)\, \Phi' \quad ; \quad 0 < i \le L \tag{5b}$$

$$S^{-1}(k+1) = A^{-2}(p_\phi^{-\frac{1}{2}} p_\phi^2)^{-1} \left\{ 1 - \left[\frac{\tilde{R}(k+1) + p_\phi^2}{\tilde{R}(k+1) + 2p_\phi} \right]^{\frac{1}{2}} \right\}, \quad p_\phi = \beta^2 P_{00}^{1,1} \tag{6}$$

where $\tilde{R}(k) = R(k)/A^2$ and the smoother error covariance matrix $P_{ii}(k+1/k+1)$ is

$$\begin{aligned}
P_{ii}(k+1/k+1) &= P_{ii}(k+1/k) - P_{i0}(k+1/k)(A\beta\ell)\, S^{-1}(k+1)(A\beta\ell)' P_{i0}'(k+1/k) \\
P_{ii}(k+1/k) &= P_{i-1,i-1}(k/k)
\end{aligned} \tag{7}$$

A. Rapprochement with Linear Theory:

Representing the bandpass additive noise $\bar{v}(k)$ in terms of its baseband quadrature components $\bar{v}_i(k)$ and $\bar{v}_q(k)$ as,

$$\bar{v}(k) = \bar{v}_i(k)\text{Cos}(\omega_c t_k + \beta\ell'\hat{x}(k)) + \bar{v}_q(k)\text{Sin}(\omega_c t_k + \beta\ell'\hat{x}(k))$$

and ignoring the $2\omega_c$ term, the phase detector output is given by

$$\eta(k+1) = A\ \text{Sin}(\beta\ell'\tilde{x}(k+1/k)) + \frac{1}{\sqrt{2}}\left[\bar{v}_i(k+1)\text{Cos}(\beta\ell'\tilde{x}(k+1/k)) - \bar{v}_q(k+1)\text{Sin}(\beta\ell'\tilde{x}(k+1/k))\right]$$

$$\tilde{x}(k+1/k) = x(k+1) - \hat{x}(k+1/k)$$

For small estimation error $\tilde{x}(k+1/k)$,

$$\eta(k+1) = \beta A\ell'\tilde{x}(k+1/k) + \frac{1}{\sqrt{2}}\bar{v}_i(k+1) \qquad (8)$$

The $\eta(k+1)$ given by (8) above is precisely the one-step ahead prediction error (innovation) for the following linear model

$$y(k+1) = \beta A\ell' x(k+1) + \frac{1}{\sqrt{2}}\bar{v}_i(k+1) \qquad (9)$$

It is easily verified that equations (3-7) reduce to the linear optimal smoother equations for the model (2,9).

B. Smoother Implementation:

Figure 1 illustrates the smoother implementation. If the various gains are replaced by their respective steady state values, the smoother consists of a sampled data phase-locked loop followed by a post-loop correction to the filtered estimates. There is an equivalent and somewhat simpler implementation to that of Figure 1. To derive this, one notes from figure 1, or the equations (3), that

$$\hat{x}(k+1-L/k+1) = \hat{x}_0(k+1-L/k+1-L) + K_L(k+1)\eta(k+1) + K_{L-1}(k)\eta(k) + \ldots + K_1(k+2-L)\eta(k+2-L) \qquad (10)$$

Under steady state conditions it is easily seen that

$$K_i = (\beta A\, S^{-1} P_F)\gamma^{i-1} \quad , \quad P_F = \lim_{k\to\infty} P_{00}(k/k)$$
$$\gamma = 1 - \beta^2 A^2 P_p\, S^{-1} \quad ; \quad P_p = \lim_{k\to\infty} P_{00}(k+1/k) \qquad (11)$$

Substitution of (11) in (10) results in the implementation shown in Figure 2. The finite impulse response filter (FIR) has output $\varepsilon(k+1)$ related to its input $\eta(k+1)$ by

$$\varepsilon(k+1) = \eta(k+1) + \gamma^{-1}\eta(k) + \ldots + \gamma^{-(L-1)}\,\eta(k+2-L) \qquad (12)$$

and ψ in Figure 2 denotes the vector

$$\psi = \beta A\, S^{-1} P_F \gamma^{L-1} \ell$$

III. Derivation of Steady State Filter/Smoother Transfer Functions and Performance Expressions

In this section we consider three specific cases of model (2). The resulting filter/smoother configurations are termed first order, second order and third order respectively. By replacing various gains and matrices by their steady-state values in equations (3-7), these difference equations are replaced by algebraic equations and may be solved explicitly for the steady state values of the filter error covariance matrix P_F, the prediction error covariance P_P, smoother error covariance P_S, etc., as in [15-17]. In the following, we consider the measurement model (9) (justified above) and replace $\beta A\ell'$ by H' for notational convenience.

A. First-Order Filter/Smoother:

In this case x is a scalar denoting the unknown phase, $\Phi = 1$ and the scalar H may be assumed to be 1 without loss of any generality. The derivations for P_P, P_F, etc., are simple for this case, one may refer to [16] for example. Substitution of these in equations (3) also yields transfer functions of the steady state filters and smoothers as in [15].

B. Second-Order Filter/Smoother:

For this case,

$$\Phi = \begin{bmatrix} 1 & T \\ 0 & 1 \end{bmatrix}, \quad H' = \beta A \begin{bmatrix} 1 & 0 \end{bmatrix} \tag{13}$$

The state vector consists of phase and frequency to be estimated. In [15-17], expressions for P_F and P_P are derived for a very specific Q matrix. Here, we also derive such expressions for any general matrix Q. This derivation is contained in Appendix B. Substitution of these and other

related parameters in (3) yields the various transfer functions associated with the steady state filters and smoothers. The detailed derivation is contained in Appendix C. The result for steady state smoother error covariance matrix is also given in Appendix B.

C. Third-Order Filter/Smoother:

For this case,

$$\Phi = \begin{bmatrix} 1 & T & T^2/2 \\ 0 & 1 & T \\ 0 & 0 & 1 \end{bmatrix} \quad ; \quad H' = \beta A \, [1 \quad 0 \quad 0] \tag{14}$$

The state vector consists of phase, frequency and the frequency derivative to be estimated. The expressions for steady-state values for various covariance matrices may be derived as for the case of first order and second order smoothers/filters. Alternatively, these are also obtainable from the simulation of the algorithm. Substitution of resulting steady-state values of Kalman gain K_i in (3) results in the transfer function of the steady-state filter/smoother as shown in Appendix C.

The above derivations are based on the assumption of a linear phase detector. The performance predicted on the basis of these expressions (Appendix B,C) is compared with simulations in the next section. As would be observed there, under the assumption of a linear phase detector, the simulation results are in close conformity with those predicted from theory.

IV. Simulation Results for Linear and Nonlinear Cases

Appendix D contains the flow chart of the simulation package developed on the VAX system for evaluating the performance of the filters/smoothers by simulations. The program includes both time domain and frequency domain analysis. Thus from the steady-state filter covariance matrices obtained from simulations, the program can also provide coefficients of various transfer functions associated with filters/smoothers for various delays and their two-sided noise bandwidths. In the following the simulation results are presented for the performance of smoothers. First we summarize the main points of these results in section V. This is then followed by a more detailed presentation in section VI.

V. Simulation Results-Summary

The simulation results obtained for a second order smoother can be broadly categorized into linear and nonlinear cases as follows.

A. Linear Cases

The first part of the simulations/computations evaluates the performance of the filter and smoother with a linear phase detector. Here we verify the results predicted from theory with those obtained from the real time covariance matrices and the simulations. The two sets of results agree within the bounds of statistical errors. Moreover from these performance plots, simple expressions for the filter/smoother noise bandwidth are also derived in terms of process noise covariance and the sampling period. This is done for both the phase and frequency estimation error variances. We consider three specific cases for the process noise variances. The first case corresponds to zero process noise. The second corresponds to nonzero process noise with its covariance known and in the

third case we consider the situation where the process noise variance is overestimated. The results show that the frequency estimation error variance is a much stronger function of the process noise than is the phase estimation error variance. Thus the noise bandwidth of the frequency estimator varies as some power ζ of noise bandwidth of the phase estimator. For the simulation examples, ζ varies between 3 to 6 for the sampling period T between 0.01s and 1s. We also establish that the asymptotic smoother improvement over the filter performance is about 5.6 dB for both the phase and frequency estimation. Another interesting result of simulations is that for phase estimation alone, a normalized (with respect to the dominant filter time constant) smoother delay of 1 is adequate to achieve asymptotic performance for the simulation examples. To improve the frequency estimates as well, the normalized delay is approximately 2.

B. Nonlinear Cases

The second part of the simulations evaluates the filter and smoother performance when the phase detector nonlinearity is taken into consideration. Here we observe that when the actual simulated process noise variance is zero but the filter/smoother is designed on the basis of nonzero process noise variance, the smoother still provides an improvement of about 5.1 dB or more when the loop SNR (linear theory) exceeds 6 dB. However for this range of loop SNR, the filter itself may result in a degradation of 1.5 dB or less due to the nonlinearity. Thus overall with the smoother and for a given value of noise bandwidth (which may be constrained from other considerations) the receiver may operate with more than 3.5 dB reduction in the carrier power to noise spectral density ratio, if the required phase error variance is about 0.1 or smaller. A similar

result is shown to be valid when the simulated process noise variance is nonzero. For the simulation example with loop SNR $\geq$ 7.5 dB, similar improvements are obtained. However, for loop SNR less than 7 dB, the smoother exhibits a very marked threshold effect in that the smoother improvement becomes small with the reduction in the loop SNR.

VI. Simulation Results-Detailed Presentation

In the following the simulation results obtained for the second-order case are presented in some detail. To be concrete we use the following often used model for the Q matrix

$$Q = \begin{bmatrix} T^2/3 & T/2 \\ T/2 & 1 \end{bmatrix} \sigma_a^2 T^2 \qquad (15)$$

One advantage of using the above Q is that the performance of the filter/smoother is then the function of only three parameters viz, σ_a $\sigma_{\bar{v}}$, and T, where $\sigma_{\bar{v}}^2 = \sigma_v^2/2$ and denotes the noise variance of $\bar{v}_i(k)/\sqrt{2}$ in the baseband model (9). We present the smoother/filter performance in terms of both the phase estimation error and frequency estimation error variances.

A. Phase Tracking Performance

First we present the results from both analysis and simulations for the case when the phase detector nonlinearity is ignored. Both the optimal filter and smoother performances are analyzed in the following.

1. Optimal Filter Performance

Here we present the performance of the optimal filter (assuming linear signal model) so as to relate these parameters to the two-sided normalized loop noise bandwidth $2B_p$, (subscript p denotes phase) a commonly used parameter in the design of phase-locked loops. In the simulations, A and β have both been normalized to 1. Thus in terms of the closed-loop transfer function matrix $G_F(Z)$ of (C8) (with $\bar{K}_3$ set equal to zero), the parameter $2B_p$ is given by,

$$2B_p = \frac{1}{2\pi j} \int_{\Gamma} G_{F,p}(z) G_{F,p}(z^{-1}) \frac{dz}{z} \qquad (16)$$

where $G_{F,p}$ represents the first component of the transfer function matrix $G_F(z)$, and Γ is some appropriate contour of integration. Figure 3 plots B_p as calculated from (16) as a function of (σ_a^2/σ_v^2) for three different values of the sampling period T viz. 0.01s, 0.1s and 1s. From these graphs it is readily seen that

$$\left.\begin{aligned} 2B_p &\cong .67(\sigma_a^2/\sigma_v^2)^{.11} T \quad ; \quad T = 1s, \ (\sigma_a^2/\sigma_v^2) \leq 10 \\ 2B_p &\cong 1.01(\sigma_a^2/\sigma_v^2)^{.226} T \quad ; \quad T = 0.1s \\ 2B_p &\cong 1.05(\sigma_a^2/\sigma_v^2)^{.25} T \quad ; \quad T = .01s \end{aligned}\right\} \qquad (17)$$

Equation (17) shows that the relation between the real two-sided bandwidth $2B_p/T$ and the parameter (σ_a^2/σ_v^2) (not a function of T) is also dependent upon the sampling period T. The last relation in (7) may be taken to be the asymptotic relation for $(2B_p/T)$ as $T \longrightarrow 0$. Figure 3 also includes the normalized loop noise bandwidth of the smoother as calculated from (16) with $G_{F,p}$ replaced by the first component of the transfer function matrix given by (C14-C16) with $\bar{K}_3=0$. Denoted by $2B_{p,S}$ this normalized bandwidth is given by,

$$2B_{p,S} \cong .28(\sigma_a^2/\sigma_v^2)^{.234} T \quad ; \ T = 0.1s \qquad (18a)$$

Comparison with the filter bandwidth of (17) yields

$$(B_p/B_{p,S}) \cong 3.6(\sigma_a^2/\sigma_v^2)^{-.008} \quad , \ T = 0.1s \qquad (18b)$$

Figure 4 plots the real two-sided noise bandwidth of the filter and

smoother denoted by $2B_{Lp}$ and $2B_{Lp,S}$ respectively where $B_{Lp} = B_p/T$ and $B_{Lp,S} = B_{p,S}/T$. The figure also plots the normalized value of the estimates of phase error variances both for the filter and smoother. These variances are the steady-state values of the (1,1) components of the actual filter error covariance P_F and the smoother error covariance matrix P_S respectively and have been obtained by simulation, with σ_{aS}^2 set equal to zero. The term $\sigma_{aS}^2 T^2$ denotes the variance of the samples of the second component of the process noise w(k) actually used in simulations. The term σ_a^2 in (15) thus represents an estimate of $\sigma_{a,S}^2$ for the purposes of filter/smoother equations (design) and thus in general σ_a^2 may be different from $\sigma_{a,S}^2$. In case the process noise covariance matrix is known precisely, then of course $\sigma_a^2 = \sigma_{a,S}^2$. As is evident from Figure 4,

$$2B_{Lp} \cong \hat{P}_F(1,1)/(\sigma_v^2 T) \quad ; \quad 2B_{Lp,S} \cong \hat{P}_S(1,1)/(\sigma_v^2 T) \tag{19}$$

where $\hat{}$ denotes estimate.

In Figure 5 we plot the normalized phase error variance for both the filter and smoother as obtained from the recursive solutions of equations (4-6). From the figure approximate expressions for these terms may be written as,

$$P_F(1,1)/(\sigma_v^2 T) \cong \begin{cases} .75(\sigma_a^2/\sigma_v^2)^{.08} & T = 1s \ , \ (\sigma_a^2/\sigma_v^2) \leq 10 \\ 1.32\ (\sigma_a^2/\sigma_v^2)^{.22} \ , & T = 0.1s \\ 1.4\ (\sigma_a^2/\sigma_v^2)^{.25} \ , & T = .01s \end{cases} \tag{20a}$$

$$P_S(1,1)/(\sigma_v^2 T) \cong .365\ (\sigma_a^2/\sigma_v^2)^{.237} \tag{20b}$$

Comparing (20) and (17,18) one observes that provided an optimum filter or smoother is used corresponding to the process noise variance σ_a^2, the maximum degradation of the phase error variance (for a specific loop noise bandwidth) due to nonzero process noise variance $\sigma_{a,S}^2 \leq \sigma_a^2$ is only about 1.34 (1.25 dB) compared to the case of $\sigma_{a,S}^2 = 0$, and this is almost independent of the variance σ_a^2.

Figure 6 provides a direct comparison of the filter performance with and without $\sigma_{a,S}^2$. This is in view of the fact that under the assumption of linear phase detection, and with $\sigma_{a,S}^2 = 0$, the phase estimation error variance $P(1,1) = (N_0 B_L/P_c)$, where P_c is the received carrier power ($P_c = A^2$ and is equal to 1 for simulations) and N_0 is the one-sided power spectral of the noise v(t) in (1). With $\sigma_v^2 = \sigma_v^2/2 = N_0/(2T)$, we have $P_F(1,1)/(\sigma_v^2 T) = 2P_F(1,1)/N_0 = 2B_L$ establishing the equivalence of the two performance measures under the assumption of $\sigma_{aS}^2 = 0$. Thus, in figure 6, the plots of $2B_L$ correspond to $P_F(1,1)/(\sigma_v^2 T)$ with $\sigma_{a,S}^2 = 0$, while those of $P_F(1,1)/(\sigma_v^2 T)$ correspond to $\sigma_{aS}^2 = \sigma_a^2$. A comparison of these two sets of curves again verifies the statement following equation (20).

In the following performance analysis of the smoother an important parameter is the optimum filter time constant τ_F. This can be easily evaluated from the filter transfer function evaluated in Appendix C and is given by

$$\tau_F = -\frac{2T}{\ell n(1-\bar{K}_1)} \tag{21}$$

where $\bar{K}_1$ denotes the first component of the normalized Kalman gain βAK_0. Figure 7 plots the normalized time constant (τ_F/T) as a function of $\sigma_a^2/\sigma_{\bar{v}}^2$. For T = 0.1s, (τ_F/T) varies between 2.5 and 14 as $(\sigma_a^2/\sigma_{\bar{v}}^2)$ varies over a large range. As is intuitively clear, higher values of σ_a^2 result in faster settling of the filter and this as shown later requires a smaller number of smoother delays to achieve the maximum possible smoother improvement. A comparison with figure 3 shows that (τ_F/T) is of the order $1/(2B_p)$.

2. Optimal Smoother Performance with Linear Phase Detector

In Figure 8 is plotted the smoother performance evaluated from simulations as a function of the smoother delay and the ratio $(\sigma_a^2/\sigma_{\bar{v}}^2)$ used in the smoother design, assuming a linear phase detector. The dotted curves in the figure plot the two-sided normalized loop noise bandwidth as computed from (16). As may be inferred from the figure, the two measures of performance are equal within the limits of statistical errors resulting due to finite data size. The minimum phase error variance (corresponding to L = ∞) varies over a range of about 0.3 to 1.4 for $(\sigma_a^2/\sigma_{\bar{v}}^2)$ between 1 to 100. It is also apparent from the figure that the amount of delay required to achieve asymptotic smoother performance has an inverse relation to $(\sigma_a^2/\sigma_{\bar{v}}^2)$. In Figure 9 is plotted the real loop noise bandwidth $2B_{Lp,S}$ as a function of normalized smoother delay (LT/τ_F), where τ_F is the time constant of the optimal filter. As is clear from the figure, the normalized value of delay required to achieve asymptotic smoother performance does not depend significantly upon $(\sigma_a^2/\sigma_{\bar{v}}^2)$.

Figures 10 and 11 plot the results similar to those of figures 8 and 9 respectively, when the actual process noise variance equals its design

value, i.e., $\sigma_{a,S}^2 = \sigma_a^2$. A comparison of these two sets of figures shows that the phase error variance can be at most 1.35 times more than for the case of $\sigma_{a,S}^2 = 0$. For intermediate values of the noise variance, $0 < \sigma_{a,S}^2 < \sigma_a^2$, the ratio would be smaller.

In figure 12, a comparison of smoother phase error variance is made for three different sampling periods T equal to .01, 0.1 and 1s respectively. As is evident from the figure, whereas the optimum filter performance is dependent upon the sampling period, the asymptotic smoother performance depends only marginally on T. Moreover as the normalized smoother delay (to achieve asymptotic performance) is almost independent of T, the actual delay L has an inverse relation to T (from Figure 7 (τ_F/T) is inversely related to T.)

3. Smoother Performance with Nonlinear Phase Detector

Figures 13-17 plot the performance of the smoother when the sinusoidal nonlinearity of the phase detector is included in the simulations. For these simulations, we consider a specific case wherein the design value of the process noise variance is equal to the measurement noise variance σ_v^2 (corresponding to a two-sided bandwidth of 1 Hz). From figure 13 it is observed that when the simulated noise variance $\sigma_{a,S}^2 = 0$, the effect of nonlinearity is to degrade the normalized phase error variance $P_S(1,1)/\sigma_v^2$ by at most a factor of 1.32 for $\sigma_v^2 \leq 2.2$ (corresponding to the filter rms phase error of 27° for a linear detector and 30° for a nonlinear phase detector).

In figure 14 is plotted the smoother performance with a nonlinear phase detector for the case of $\sigma_{a,S}^2 = \sigma_a^2$. Here the variation of

normalized phase estimation error variance depends much more strongly on σ_v^2. For $\sigma_v^2 < 1.4$ (corresponding to a rms phase error of 28.5° at the phase detector output), the degradation is within a factor of 1.7 (2.3 dB). The degradation can be much higher for larger values of σ_v^2. Figure 15 plots the phase error variance normalized by the sampling period T vs the normalized smoother delay. Such a normalized result is expected to be approximately valid for different values of T.

Figures 16 and 17 compare the filter and the limiting smoother performance as a function of optimal filter performance with a linear phase detector. Thus the inverse of the phase error variance of the filter with nonlinearity vs 10 log (P_c/N_0B_L) = 10 log $(1/\sigma_\phi^2)$ is plotted in figure 16 for the case of $\sigma_{a,S}^2 = 0$. Here, σ_ϕ^2 denotes the phase error variance of a phase-locked loop with a linear phase detector and having a loop noise bandwidth of B_L Hz and (P_c/N_0) is the receiver carrier power to noise spectral density ratio. Figure 16 also plots the corresponding results for the smoother with and without nonlinearity. As may be inferred from the figure, for the case of a linear phase detector, the smoother provides an improvement of 5.6 dB over the filter. When the phase detector nonlinearity is taken into consideration, then for a range of 10 log $(1/\sigma_\phi^2) \geq 6$ dB, the smoother still provides an improvement of at least 5.1 dB over the filter. Note, however, that the filter performance can itself be degraded by as much as 1.5 dB due to phase detector nonlinearity. Since the plots in figure 16 correspond to a fixed value of B_L, these results indicate that with a smoother, the receiver can be operated with at least 3.5 dB smaller (P_c/N_0) ratio when it is desired to have a 0.1 or smaller value for the phase error variance.

Figure 17 plots the corresponding results for the case of $\sigma_{a,S}^2 = \sigma_a^2$. Here it is observed that the effects of nonlinearity are more dominant resulting in a threshold behavior in the smoother phase error variance. However, for 10 log $(P_c/N_0B_L) \geq 7.5$ dB, the results in terms of smoother performance are close to those for the case of $\sigma_{a,S}^2 = 0$.

B. Frequency Tracking Performance

In the following we present the performance of the filter and smoother in terms of the frequency estimation error.

1. Optimal Filter Performance

The frequency estimation error variance is presented in terms of the frequency tracking loop's normalized two-sided loop-noise bandwidth denoted by $2B_f$. This parameter can also be computed from (16) with $G_{F,p}$ replaced by $G_{F,f}$ - the second component of the transfer function matrix $G_F(z)$. The actual two-sided loop bandwidth $2B_{Lf}$ equals $(2B_f/T)$ or is equivalently given by $P_F(2,2)/(\sigma_v^2 T)$. This parameter is plotted vs the design parameter (σ_a^2/σ_v^2) for the case of $\sigma_{a,S}^2 = 0$ in figure 18. From these graphics it is readily seen that approximately,

$$\left.\begin{aligned} 2B_{Lf} &\cong 0.32\,(\sigma_a^2/\sigma_v^2)^{.64} \quad , \; T = 1s \; , \; (\sigma_a^2/\sigma_v^2) \leq 10 \\ 2B_{Lf} &\cong 0.35\,(\sigma_a^2/\sigma_v^2)^{.75} \quad ; \; T = 0.1s \end{aligned}\right\} \qquad (22)$$

A comparison of (22) with (19,20) shows that approximately

$$\left.\begin{aligned} 2B_{Lf} &\cong 10\,(2B_{Lp})^{5.8} \quad , \; T = 1s \; , \; (\sigma_a^2/\sigma_v^2) \leq 10 \\ 2B_{Lf} &\cong .34\,(2B_{Lp})^{3.32} \quad , \; T = 0.1s \\ 2B_{Lf} &\cong .30\,(2B_{Lp})^{3} \quad , \; T = .01s \end{aligned}\right\} \qquad (23)$$

It is hardly surprising that for low values of T, the frequency estimation error variance is proportional to the third power of $2B_p$. Still more important is the fact that the frequency estimation error degrades at a much faster rate with B_{Lp} as T is increased.

2. Optimal Smoother Performance with Linear Phase Detector

In figure 18 is also plotted the equivalent loop noise bandwidth of the smoother $2B_{Lf,S} = P_S(2,2)/(\sigma_v^2 T)$ for the case of T = 0.1s. This result can be approximated by the following expression.

$$2B_{Lf,S} = .097\ (\sigma_a^2/\sigma_v^2)^{0.72} \tag{24}$$

A comparison with (22) shows that the ratio of B_{Lf} to $B_{Lf,S}$ is given by $3.6(\sigma_a^2/\sigma_v^2)^{0.03}$ which for low values of (σ_a^2/σ_v^2) is approximately 5.6 dB.

Figures 19 and 20 plot the normalized frequency estimation error variance for the smoother as a function of smoother delay corresponding to $\sigma_{a,S}^2 = 0$ and $\sigma_{a,S}^2 = \sigma_a^2$, respectively. Comparison with figures 9 and 11 respectively shows that the smoother delay required to achieve the asymptotic improvement in frequency estimation is about two times that required for phase estimation alone. Even so, a normalized delay of less than two is adequate for realizing the asymptotic improvement. Also, as already discussed, the frequency estimation error variance is a much stronger function of (σ_a^2/σ_v^2) and the actual process noise variance $\sigma_{a,S}^2$.

3. Smoother Performance with Nonlinear Phase Detector

In figure 21 is plotted the normalized frequency estimation error

variance for the case of $\sigma_a^2 = \sigma_{\bar{v}}^2$ and the actual process noise variance $\sigma_{a,S}^2 = 0$. For $\sigma_{\bar{v}}^2 \leq 2.2$, the filter and smoother performances are degraded by a factor of 1.18 and 1.24 respectively. Figure 22 plots the smoother performance for the case of $\sigma_{a,S}^2 = \sigma_a^2$.

C. Smoother Parameters

Figures 23 and 24 plot both components of the asymptotic smoother gain $K_i(k)$ as $k \to \infty$ (see equation (4)) for various values of the delay variable i, corresponding to two different values of the design parameter ($\sigma_a^2/\sigma_{\bar{v}}^2$). As is apparent from the figures, the smoother gain is negligibly small for $i > 20$ in both of these cases.

VII. Conclusions and Suggestions for Further Work

The report has presented the performance of the suboptimal filter and smoother for the phase and frequency estimation of a sinusoid under the presence of both the process noise and observation noise. The performance predicted on the basis of linear estimation theory is in close proximity with the corresponding results obtained with simulations, when the phase detector is assumed linear. Such simulation results are applicable when the phase detector nonlinearity is taken into consideration and the receiver is operating under high signal-to-noise ratio conditions. Under such conditions, the smoother improves both the phase and frequency estimation errors as compared to the filter by about 5.6 dB.

However, as the signal-to-noise ratio is reduced, the corresponding improvement is also reduced. Also, such a difference is more severe when the process noise is present than when only the observation noise is present. In the presence of both the nonlinearity and the process noise, the smoother performance exhibits a marked threshold behavior, in that the smoother performance degrades rapidly with decrease in 10 log $(1/\sigma_\phi^2)$ below 7.5 dB. However, for 10 log $(P_c/N_0B_L) \geq 7.5$ dB, the results in terms of smoother performance are close to those for the case of $\sigma_{a,S}^2 = 0$.

From the simulation examples it also appears that the performance of the filter/smoother does not change very significantly if the actual process noise variance is smaller than its design value.

Although not studied in this report, it is expected that the degradation caused by ignoring the process noise variance completely or by underestimating it in the design would be relatively much more severe. Thus in situations where the process noise variance is not known, an upper

bound for it should be used in the design. This however, can lead to much higher estimation error than the minimum possible value as it follows from the simulations (the actual phase error variance would be close to the value obtained when the actual process noise variance is equal to its bound).

Therefore, for the future research we propose an adaptive implementation which either explicitly or implicitly estimates the actual process noise variance.

Acknowledgement: The author acknowledges a partial support provided by the California State University, Long Beach in the form of Faculty Research Award.

References

[1] D.C. Youla, "The Use of the Method of Maximum Likelihood in Estimating Continuous-Modulated Intelligence Which has been Corrupted by Noise," IRE Trans. Inform. Theory, Vol. PGIT-3, pp. 90-105, March 1954.

[2] H.L. Van Trees, "Analog Communication Over Randomly-Time-Varying Channels," IEEE Trans. Inform. Theory, Vol. IT-12, pp. 51-63, January 1966.

[3] A.J. Viterbi, "On the Minimum Mean Square Error Resulting from Linear Filtering of Stationary Signals in White Noise," IEEE Trans. Inform. Theory, Vol. IT-11, pp. 594-595, October 1965.

[4] H.L. Van Trees, "Application of State-Variable Techniques in Detection Theory," Proc. IEEE, Vol. 58, pp. 653-669, May 1970.

[5] D.L. Snyder, The State Variable Approach to Analog Communication. Cambridge, Mass.; MIT Press, 1971.

[6] R.E. Kalman and R.S. Bucy, "New Results in Linear Filtering and Prediction Problems," J. Basic Eng., Ser. D, Vol. 83, pp. 95-108, March 1961.

[7] C.N. Kelly and S.C. Gupta, "Discrete-Time Demodulation of Continuous-Time Signals," IEEE Trans. Inform. Theory, Vol. IT-18, pp. 488-493, July 1972.

[8] A.M. Jazwinski, Stochastic Processes and Filtering Theory, Academic Press, New York, 1970.

[9] S. Prasad and A.K. Mahalanabis, "Finite Lag Receivers for Analog Communication," IEEE Trans. Comm., Vol. COM-23, pp. 204-211, February 1975.

[10] J.B. Moore, "Discrete-Time Fixed-Lag Smoothing Algorithms," Automatica, Vol. 9, pp. 163-173, 1973.

[11] J.S. Meditch, "Orthogonal Projection and Discrete Optimal Linear Smoothing," SIAM J. Control, Vol. 5, pp. 74-78, 1967.

[12] J.S. Meditch, Stochastic Optimal Linear Estimation and Control, McGraw-Hill, New York, 1969.

[13] B.D.O. Anderson and J.B. Moore, Optimal Filtering, Prentice-Hall, New Jersey, 1979.

[14] K.K. Biswas and A.K. Mahalanabis, "Suboptimal Algorithms for Nonlinear Smoothing," IEEE Trans. Aerosp. Electron. Syst., Vol. AES-9, pp. 529-534, July 1973.

[15] C.A. Pomalaza Raez and W.J. Hurd, "Improved Carrier Tracking by Smoothing Estimates," IEEE Trans. Aerosp. Electron. Syst., Vol. AES-21, pp. 610-618, Sept. 1985.

[16] B. Ekstrand, "Analytical Steady-State Solutions for Kalman Tracking Filter," IEEE Trans. on Aerosp. Electron. Syst., Vol. 19, pp. 815-819, November 1983.

[17] B. Friedland, "Optimum Steady-State Positions and Velocity Estimation Using Noisy Sampled Position Data," IEEE Trans. Aerosp. Electron. Syst., Vol. 9, pp. 906-911, November 1973.

Appendix A: Smoother Equations

In the following, the filter and smoother equations are presented which result by expanding the nonlinear measurement function h(x,k) into a Taylor series around the predicted estimate of x(k) and retaining only the linear and quadratic terms. Much of the simplicity in the resulting equations is due to the fact that $2\omega_c t$ and higher order harmonic terms are ignored. These harmonic terms result from the quadratic terms present in the filter/smoother equations.

Denoting by h(x,k) the function A Sin($\omega_c t_k + \beta \ell' x(k)$) and by $h_x(x,k)$ its partial derivative with respect to x, the smoother equations can be decomposed into two sets of equations termed filter equations and "smoother" equations as follows. Letting $x_i(k) \triangleq x(k-i)$, $\hat{x}_i(k/j)$ denote the estimate of $x_i(k)$ on the basis of observations up to time j, one obtains [7-9]:

Filter State Equations:

$$\hat{x}_0(k+1/k+1) = \Phi\hat{x}_0(k/k) + M_0(k+1)\nu(k+1) \qquad (A1)$$

$$\nu(k+1) = y(k+1) - h(\hat{x}(k+1/k),\ k+1) \qquad (A2)$$

where $M_0(k+1)$ is the filter gain.

Smoother State Equations:

$$\hat{x}_i(k+1/k+1) = \hat{x}_{i-1}(k/k) + M_i(k+1)\nu(k+1),\ 0 < i \leq L \qquad (A3)$$

where L denotes the smoother delay.

Filter/Smoother Gain:

$$M_i(k+1) = P_{i0}(k+1/k)\ h_x'\sigma^{-1}(k+1),\ 0 \leq i \leq L \qquad (A4)$$

Error Covariance Update:

In (A4) $P_{i0}\ (k/j)$ denotes $E\left[\left\{x(k-i) - \hat{x}(k-i/j)\right\}\ \left\{x(k) - \hat{x}(k/j)^T\right\}\right]$ with j = k-1. A recursive update for $P_{i0}\ (k/k)$ is given as

$$P_{i0}(k+1/k+1) = P_{i0}(k+1/k) - [P_{i0}(k+1/k)h_x']\sigma^{-1}(k+1)\,[P_{00}(k+1/k)h_x']^T \quad (A5)$$

$$P_{i0}(k+1/k) = P_{i-1,0}(k/k)\Phi^T \quad , \; 0 < i \leq L \quad (A6)$$

$$\sigma(k) = h_x P_{00}(k/k-1)h_x' + R(k) + \frac{1}{2}\sum_{i,j=1}^{n}\sum_{r,s=1}^{n} P_{00}^{i,r}\,P_{00}^{s,j}\,\frac{\partial^2 h}{\partial x^i \partial x^s}\,\frac{\partial^2 h}{\partial x^r \partial x^j} \quad (A7)$$

In equation (A7) x^i denotes the ith component of x and P_{00}^{ij} denotes (i,j)th component of the matrix P_{00}. The smoothing error covariance matrix $P_{ii}(k/k) = E\left\{\tilde{x}(k-i/k)\tilde{x}^T(k-i/k)\right\}$, $\tilde{x}(k-i/k) = x(k-i) - \hat{x}(k-i/k)$, is given by

$$P_{ii}(k+1/k+1) = P_{ii}(k+1/k) - P_{i0}(k+1/k)\,h_x'\,\sigma^{-1}(k+1)h_x\,P_{i0}'(k+1/k); 0 \leq i \leq L$$

$$P_{ii}(k+1/k) = P_{i-1,i-1}(k/k), \quad 1 \leq i \leq L \quad (A8)$$

To specialize the algorithm to the signal model (1,2), h_x and h_{xx} are evaluated as,

$$h_x = A\sqrt{2}\,\ell'\,\mathrm{Cos}\,(\hat{\theta}(k)); \quad \frac{\partial^2 h}{\partial x^2} = A\sqrt{2}\,\ell\ell'\,\mathrm{Sin}\,(\hat{\theta}(k));$$

$$\hat{\theta}(k) \triangleq \omega_c t_k + \beta\ell'\hat{x}(k/k-1) \quad (A9)$$

$$\sigma^{-1}(k) = \left\{2p_\phi A^2\,\mathrm{Cos}^2(\hat{\theta}(k)) + R(k) + p_\phi^2 A^2\,\mathrm{Sin}^2(\Theta(k))\right\}^{-1}, \; p_\phi = \ell' P_{00}\ell = P_{00}^{1,1}(k/k-1) \quad (A10)$$

The above expression for $\sigma^{-1}(k)$ may easily be reorganized as

$$\sigma^{-1}(k) = A^{-2}\left[p_\phi + \tfrac{1}{2}p_\phi^2 + \tilde{R}(k)\right]^{-1}\left[1 + d(k)\mathrm{Cos}(2\hat{\theta}(k))\right]^{-1} \quad (A11)$$

$$d(k) \triangleq \frac{p_\phi - \tfrac{1}{2}p_\phi^2}{p_\phi + \tfrac{1}{2}p_\phi^2 + \tilde{R}(k)} \; ; \; \tilde{R}(k) = R(k)/A^2$$

Expansion of the second term on the right hand side into a cosine Fourier series results in

$$\sigma^{-1}(k) = A^{-2}\left[p_\phi + \tfrac{1}{2}p_\phi^2 + \tilde{R}(k)\right]^{-1}\left\{a_0 + a_1\cos(2\hat{\theta}(k)) + \ldots\right\} \qquad \text{(A12)}$$

where a_0, a_1, etc., are the Fourier series coefficients. Thus

$$a_0 = \frac{1}{\pi}\int_0^{\pi}\frac{dx}{1+d(k)\cos x} = \frac{1}{\sqrt{1-d^2(k)}}$$

$$a_1 = \frac{2}{\pi}\int_0^{\pi}\frac{\cos x\,dx}{1+d(k)\cos x} = \frac{2}{d(k)}\left\{1 - \frac{1}{\sqrt{1-d^2(k)}}\right\} \qquad \text{(A13)}$$

Substitution of $\sigma^{-1}(k)$ from (A12,A13) into (A4) results in

$$M_i(k+1) = P_{i0}(k+1/k)A\sqrt{2}\,\ell\left[p_\phi + \tfrac{1}{2}p_\phi^2 + \tilde{R}(k+1)\right]^{-1} A^{-2}\left\{C_1\cos(\hat{\theta}(k)) + C_3\cos(3\hat{\theta}(k)) + \ldots\right\}$$

with

$$C_1 = a_0 + \frac{a_1}{2} = \frac{1}{d(k)}\left\{1 - \left[\frac{1-d(k)}{1+d(k)}\right]^{\frac{1}{2}}\right\} \qquad \text{(A14)}$$

Recognizing that $P_{i0}(k+1/k)$ is baseband, the baseband part of the correction term in (A2,A3) may be written as

$$M_i(k+1)\nu(k+1) = K_i(k+1)\eta(k+1)$$

$$K_i(k+1) = A\,P_{i0}(k+1/k)\,C_1\left[A^2p_\phi + \tfrac{1}{2}A^2p_\phi^2 + R(k+1)\right]^{-1}$$

$$\eta(k+1) = \sqrt{2}\,y(k+1)\cos(\hat{\theta}(k+1)) \qquad \text{(A15)}$$

In (A15) $K_i(k+1)$ is baseband, and the term $M_i(k+1)\sin(\hat{\theta}(k+1))$ has been ignored as this does not contribute any baseband component.

Similarly, the second term on the right hand side of (A8) is given by

$$P_{i0}(k+1/k)\ell\ell' P_{i0}(k+1/k)\,A^2\left[1 + \cos(2\hat{\theta}(k+1))\right]\left[A^2p_\phi + \frac{1}{2}A^2p_\phi^2 + R(k+1)\right]^{-1}\left\{a_0 + a_1\cos(2\hat{\theta}(k+1)) + \ldots\right\}$$

and its baseband part is simply

$$P_{i0}(k+1/k)(A\beta\ell)(A\beta\ell)'P_{i0}(k+1/k)\left[A^2P_\phi + \tfrac{1}{2}A^2p_\phi^2 + R(k+1)\right]^{-1}(a_0 + a_1/2) \quad (A16)$$

Appendix B: Steady State Performance Equations for a Second Order Linear Filter/Smoother

Denoting by $\bar{R}$, the variance of the additive noise term $\frac{1}{\sqrt{2}}\bar{v}_i(k+1)$ in equation (8), the steady-state error covariance matrix P_p is the solution of the following algebraic Riccati equation.

$$P_p = \Phi\left[P_p - P_pH(H'P_pH + \bar{R})^{-1}H'P_p\right]\Phi' + Q \tag{B1}$$

or

$$P_p - P_pH(H'P_pH + \bar{R})^{-1}H'P_p = \Phi^{-1}(P_p - Q)(\Phi')^{-1} \tag{B2}$$

Denoting by P_{ij} the ij th component of P_p, the left hand side of (B2) denoted B equals,

$$B = \frac{1}{(P_{11} + \bar{R})}\begin{bmatrix} P_{11}\bar{R} & P_{12}\bar{R} \\ P_{12}\bar{R} & (P_{11}P_{22} - P_{12}^2) + P_{22}\bar{R} \end{bmatrix} \tag{B3}$$

Letting A denote the matrix on the right hand side of (B2), one obtains

$$\left.\begin{aligned} A_{11} &= (P_{11} - 2TP_{12} + T^2P_{22}) - \bar{Q}_{11} \quad ; \qquad \bar{Q}_{11} = Q_{11} - 2TQ_{12} + T^2Q_{22} \\ A_{12} &= (P_{12} - TP_{22}) - \bar{Q}_{12} \quad ; \quad \bar{Q}_{12} = Q_{12} - TQ_{22} \\ A_{22} &= P_{22} - \bar{Q}_{22} \quad ; \quad \bar{Q}_{22} = Q_{22} \end{aligned}\right\} \tag{B4}$$

Substitution of (B3) and (B4) results in the following set of equations in P_{11}, P_{12} and P_{22}.

$$P_{11}\,\bar{R} = (P_{11} + \bar{R})\,\left\{P_{11} - 2TP_{12} + T^2 P_{22} - \bar{Q}_{11}\right\} \tag{B5}$$

$$P_{12}\,\bar{R} = (P_{11} + \bar{R})\,\left\{P_{12} - T\,P_{22} - \bar{Q}_{12}\right\} \tag{B6}$$

$$(P_{11}\,P_{22} - P_{12}^2) + P_{22}\,\bar{R} = (P_{11} + \bar{R})\,(P_{22} - \bar{Q}_{22}) \tag{B7}$$

Equation (B7) can also be written as

$$\bar{Q}_{22}\,P_{11} - P_{12}^2 + \bar{R}\,\bar{Q}_{22} = 0 \tag{B8}$$

or

$$P_{11} + \bar{R} = P_{12}^2/\bar{Q}_{22} \tag{B'8}$$

Substitution of $(P_{11} + \bar{R})$ from (B'8) into (B6) and a little simplification yields

$$P_{12} - T\,P_{22} = \bar{Q}_{12} + \bar{R}\,\frac{\bar{Q}_{22}}{P_{12}} \tag{B9}$$

Substitution of (B9) and (B'8) in equation (B5) results in the following algebraic equation in P_{12}.

$$\frac{P_{12}^4}{\bar{Q}_{22}^2} - \frac{T}{\bar{Q}_{22}}\,P_{12}^3 - \left\{2\bar{R} + T\,\bar{Q}_{12} + \bar{Q}_{11}\right\}\frac{P_{12}^2}{\bar{Q}_{22}} - T\,\bar{R}\,P_{12} + \bar{R}^2 = 0 \tag{B10}$$

Defining $\tilde{P}_{12} \triangleq P_{12}/\sqrt{\bar{Q}_{22}\,\bar{R}}$, then substitution of $\bar{Q}_{11}$, $\bar{Q}_{22}$, $\bar{Q}_{12}$ in terms of Q_{11} etc. from (B4) results in the following equation for $\tilde{P}_{12}$,

$$\left.\begin{aligned} &\tilde{P}_{12}^4 - a\,\tilde{P}_{12}^3 - (2 + b)\,\tilde{P}_{12}^2 - a\,\tilde{P}_{12} + 1 = 0 \\ &a = T\sqrt{Q_{22}/\bar{R}} \quad ; \quad b = \frac{Q_{11} - TQ_{12}}{\bar{R}} \end{aligned}\right\} \tag{B11}$$

In terms of the solution $\tilde{P}_{12}$ of (B11), the elements of the matrix P_p can be computed as follows.

$$
\begin{aligned}
P_{12} &= \sqrt{Q_{22}\,\bar{R}}\;\tilde{P}_{12} \\
P_{11} &= \bar{R}\,(\tilde{P}_{12}^2 - 1) \\
P_{22} &= \sqrt{\frac{Q_{22}\,\bar{R}}{T}}\left\{\tilde{P}_{12} - \frac{1}{\tilde{P}_{12}}\right\} + \left(Q_{22} - \frac{Q_{12}}{T}\right)
\end{aligned}
\tag{B12}
$$

Due to symmetry in the coefficients of the polynomial in equation (B11), it can be factorized as

$$(\tilde{P}_{12}^2 - C_1\,\tilde{P}_{12} + 1)\;(\tilde{P}_{12}^2 - C_2\,\tilde{P}_{12} + 1)$$

comparing the coefficients yields the solution for C_1 and C_2 as follows,

$$C_{1,2} = \tfrac{1}{2}\left[a \pm \sqrt{a^2 + 4\,(4 + b)}\right] \tag{B13}$$

Thus for the existence of the solution, one must satisfy the condition

$$a^2 + 4\,(4 + b) > 0 \tag{B14}$$

Now $\tilde{P}_{12}$ is the solution of

$$\tilde{P}_{12}^2 - C\,\tilde{P}_{12} + 1 = 0 \tag{B15}$$

Since it is required that $|\tilde{P}_{12}| > 1$ (note that the solutions of (B15) are λ and λ^{-1} for some real λ) ;

$$
\begin{aligned}
\tilde{P}_{12} &= \tfrac{1}{2}\left[C + \sqrt{C^2 - 4}\;\right]; \qquad C > 0 \\
&= \tfrac{1}{2}\left[C - \sqrt{C^2 - 4}\;\right]; \qquad C < 0
\end{aligned}
\tag{B16}
$$

For the above solution to exist $C^2 > 4$. If only one solution of (B13) satisfies this condiition then the solution is uniquely determined. This

would be the case, for example, when

$$|4 + b| < 4 \qquad \text{or} \qquad -8 < b < 0 \tag{B17}$$

If on the other hand both solutions of (B13) satisfy $C^2 > 4$, then the one satisfying $P_{22} > Q_{22}$ ($P^F{}_{22} + Q_{22} = P^P{}_{22}$) where superscripts F and P stand for filter and predictor respectively is the desired solution.

With the knowledge of P_p, the steady-state filter error covariance matrix P_F is simply given as

$$P_F = P_p - P_p H\,(H' P_p H + \bar{R})^{-1} H' P_p$$

The smoother covariance matrix P_{i0} and the filter smoother gains K_i can then be obtained from equations (C10-C13) of the Appendix C, which are time invariant versions of the relevant smoother equations. Moreover, the smoother performance for various values of the delay can be evaluated recursively from equation (7). Equivalently the asymptotic performance of the smoother can be evaluated from the following nonrecursive equation.

$$\left.\begin{aligned} &(P_p - P_S) - P_p \tilde{\Phi}' P_p^{-1} (P_p - P_S) P_p^{-1} \tilde{\Phi} P_p = P_p - P_F \\ &\text{where} \\ &\tilde{\Phi} = \Phi - K_0 H' \quad ; \quad P_S = \lim_{L\to\infty} \lim_{k\to\infty} P_{LL}(k/k) \end{aligned}\right\} \tag{B18}$$

Letting,

$$P_p \tilde{\Phi}' P_p^{-1} = \begin{bmatrix} \alpha & \gamma \\ \beta & \delta \end{bmatrix}$$

then the solution for $\tilde{P}_S \triangleq (P_p - P_S)$ is given in terms of $\tilde{P}_F \triangleq (P_p - P_F)$ as follows,

$$\begin{bmatrix} \tilde{P}_S(1,1) \\ \tilde{P}_S(1,2) \\ \tilde{P}_S(2,2) \end{bmatrix} = \begin{bmatrix} (1-\alpha^2) & -2\alpha\gamma & -\gamma^2 \\ -\alpha\beta & 1-(\alpha\delta+\beta\gamma) & -\gamma\delta \\ -\beta^2 & -2\beta\delta & 1-\delta^2 \end{bmatrix}^{-1} \begin{bmatrix} \tilde{P}_F(1,1) \\ \tilde{P}_F(1,2) \\ \tilde{P}_F(2,2) \end{bmatrix} \qquad \text{(B19)}$$

Appendix C: Transfer functions of the steady-state filter/smoother.

Third-Order Filter:

From equations (2), (3), (8) and under the assumption of a linear phase detector, one obtains

$$\hat{x}(k+1/k+1) = \Phi\ \hat{x}(k/k) + K_0 A\beta\ell'\Phi\{\ x(k) - \hat{x}(k/k)\} + K_0 A\beta\ell' w(k) + K_0 v_i(k+1) \qquad (C1)$$

In equation (C1), $v_i(k+1) \triangleq \frac{1}{\sqrt{2}}\bar{v}_i(k+1)$, and $\{w(k\}$ is a vector white Gaussian noise process as appearing in equation (2). Subtraction of (C1) from the second of equations (2) yields the following equation after some simplification and taking the Z transform on both sides of the equation.

$$\{zI - (I - \bar{K}\ell')\ \Phi\}\tilde{X}^F(z) = [I - \bar{K}\ell']W(z) - K_0 z V_i(z) \qquad (C2)$$

In equation (C2) above, $\bar{K} \triangleq \beta A K_0 = [\bar{K}_1\ \bar{K}_2\ \bar{K}_3]'$ and $\tilde{X}^F(z), W(z)$ and $V_i(z)$ represent the Z transforms of $\tilde{x}(k/k)$, $w(k)$ and $v_i(k)$ respectively. Letting the vector function $\zeta(z)$ represent the right hand side of (C2), the equation (C2) may be written as a set of following three equations in the unknowns $\tilde{X}_1(z)$, $\tilde{X}_2(z)$ and $\tilde{X}_3(z)$ (after substitution of Φ from (14)).

$$[z - (1-\bar{K}_i)]\ \tilde{X}_1^F - (1-\bar{K}_1)T\ \tilde{X}_2^F - (1-\bar{K}_1)\frac{T^2}{2}\ \tilde{X}_3^F = \zeta_1(z) \qquad (C3,1)$$

$$\bar{K}_2\ \tilde{X}_1^F + [z - (1-\bar{K}_2 T)]\ \tilde{X}_2^F - T(1-\bar{K}_2 T/2)\ \tilde{X}_3^F = \zeta_2(z) \qquad (C3,2)$$

$$\bar{K}_3\ \tilde{X}_1^F + \bar{K}_3 T\ \tilde{X}_2^F + [z - (1-\bar{K}_3 T^2/2)]\tilde{X}_3^F = \zeta_3(z) \qquad (C3,3)$$

The set of equations (C3) can be solved to obtain the following transfer function matrix between $V_i(z)$ and $\tilde{X}^F(z)$ (setting $W(z)\equiv 0$) ,

$$\frac{A\beta\tilde{X}^F(z)}{zV_i(z)} = \frac{-1}{D(z)} \begin{bmatrix} \bar{K}_1(z-1)^2 + (\bar{K}_2T + \tfrac{1}{2}\bar{K}_3T^2)(z-1) + \bar{K}_3T^2 \\ (z-1)\left[\bar{K}_2(z-1) + \bar{K}_3T\right] \\ (z-1)^2\,\bar{K}_3 \end{bmatrix} \qquad (C4)$$

$$D(z) = (z-1)^3 + (\bar{K}_1 + \bar{K}_2T + \bar{K}_3\frac{T^2}{2})(z-1)^2 + (\bar{K}_2T + \frac{3}{2}\bar{K}_3T^2)(z-1) + \bar{K}_3T^2 \qquad (C5)$$

From (14) and (C5) it follows that

$$\frac{A\beta\ell'\Phi\,\tilde{X}^F(z)}{zV_i(z)} = \frac{-1}{D(z)}\left\{(\bar{K}_1+\bar{K}_2T+\bar{K}_3\frac{T^2}{2})(z-1)^2 + (\bar{K}_2T+\frac{3}{2}\bar{K}_3T^2)(z-1) + \bar{K}_3T^2\right\} \qquad (C6)$$

From equation (8), in the absence of process noise w(k), the transfer function between $\eta(k+1)$ and $v_i(k+1)$, (or between $\eta(k+1)$ and $y(k+1)$) is given by

$$\frac{\eta(z)}{V_i(z)} = 1 - \frac{A\beta\ell'\Phi\,\tilde{X}^F(z)}{zV_i(z)} = (z-1)^3/D(z) \qquad (C7)$$

By exploiting the linear property of the filter (or smoother) and considering the case when $w(k) = 0$ ($x(k) \equiv 0$, implying that $\tilde{x}(k/k) = -\hat{x}(k/k)$), one readily observes that the filter transfer function between $y(k)$ and $\hat{x}(k/k)$ (or between $v_i(k)$ and $\hat{x}(k/k)$) is given by

$$A\beta G_F(z) \triangleq A\beta\frac{\hat{X}^F(z)}{Y(z)} = \frac{z}{D(z)} \begin{bmatrix} \bar{K}_1(z-1)^2 + (\bar{K}_2T+\tfrac{1}{2}\bar{K}_3T^2)(z-1) + \bar{K}_3T^2 \\ (z-1)\left[\bar{K}_2(z-1) + \bar{K}_3T\right] \\ (z-1)^2\,\bar{K}_3 \end{bmatrix} \qquad (C8)$$

The first term of the transfer function matrix on the right hand side of (C8) is simply A times the transfer function between the phase estimate and the input signal y(k). Similarly the second term represents A times the transfer function between the frequency estimate and the input and so on. Using frequency domain techniques, these transfer functions are used in the developed software to evaluate the filter loop noise bandwidth.

Transfer Function of Third-Order Smoother:

It is easily seen from equation (3) that the smoothed estimate (with smoother lag equal to L) of x(k+1-L) may be written as,

$$\hat{x}(k+1-L/k+1) = \hat{x}(k+1-L/k+1-L) + K_L(k+1)\eta(k+1) + K_{L-1}(k)\eta(k) + \ldots + K_1(k+2-L)\eta(k+2-L) \tag{C9}$$

The various smoother gains and the covariance matrices are now replaced by their respective steady-state values as follows. From equations (4) and (5) one obtains

$$P_{i0}(k+1/k) = P_{i-1,0}(k/k-1)\tilde{\Phi}'(k) \tag{C10}$$

where

$$\tilde{\Phi}(k) = \Phi(k) - A\beta\Phi(k)K_0(k)\ell' \tag{C11}$$

A nonrecursive solution of (C10) under steady state can be obtained by replacing $\tilde{\Phi}(k)$ and $P_{00}(k/k-1)$ by their steady-state values denoted by $\tilde{\Phi}$ and P_p respectively. Thus,

$$\lim_{k \to \infty} p_{i0}(k+1/k) = p_p\left[\tilde{\Phi}'\right]^i \quad ; \quad 1 \le i \le L \tag{C12}$$

$$\lim_{k \to \infty} K_i(k+1) = A\beta P_p\left[\tilde{\Phi}'\right]^i \ell S^{-1} \tag{C13}$$

Denoting by $\tilde{X}^S$ the Z transform of the smoother estimation error $\tilde{x}(k+1-L/k+1)$, then the substitution of (C13) and taking the Z transform of the resulting error equation yield,

$$-A\beta \frac{\hat{X}^S(z)}{V_i(z)} = A\beta \frac{\tilde{X}^S(z)}{V_i(z)} = A\beta \frac{\tilde{X}^F(z)}{V_i(z)} z^{-(L-1)} - (A\beta)^2 S^{-1} P_p\left[\tilde{\Phi}'\right]^L \frac{n(z)}{V_i(z)} \tag{C14}$$
$$\times \left\{ I + (\tilde{\Phi}')^{-1} z^{-1} + \ldots + (\tilde{\Phi}')^{-(L-1)} z^{-(L-1)} \right\} \ell$$

Substitution of (C6) and (C7) into (C14) yields $\tilde{X}^S(z)/V_i(z)$ or $-\hat{X}^S(z)/V_i(z)$ (taking $x(k) \equiv 0$). Equation (C14) in its present form is more convenient for computer evaluation of the transfer functions and has been used for such purposes in the program SIM. However by summing up the terms in the finite series in (C14), the second term on the right hand side of (C14) may be written as,

$$A\beta\, z^{-(L-1)} (z-1)^3 S^{-1} P_p \tilde{\Phi}' (I - \tilde{\Phi}' z)^{-1} \left\{ I - \left[\tilde{\Phi}\right]^L z^L \right\} \ell / D(z) \tag{C15}$$

In particular, the transfer function between the smoothed phase estimate $\hat{\theta}^S(k)$ and $v_i(k)$ (or $y(k)$) obtained by premultiplying (C14) by ℓ' is given by

$$\frac{\hat{\theta}^S(z)}{V_i(z)} = \frac{1}{A} z^{-(L-1)} \left\{ \bar{K}_1 (z-1)^2 + (\bar{K}_2 T + \tfrac{1}{2} \bar{K}_3 T^2)(z-1) + \bar{K}_3 T^2 \right.$$
$$\left. + (z-1)^3 \ell' \{I - \tilde{\Phi}^L z^L\} \{I - \tilde{\Phi} z\}^{-1} \tilde{\Phi} \bar{K}_0 \right\} / D(z) \tag{C16}$$

Transfer functions to the smoothed estimates of the frequency and frequency

rate can be similarly obtained.

First and Second Order Filter/Smoothers:

The results derived for the third order filter/smoother can be directly specialized to obtain the corresponding results for lower order estimators. For example, substitution of $\bar{K}_3 = 0$ in equations (C4), (C5) and considering only the first two components of $\tilde{X}^F$ result in

$$\frac{A\beta\tilde{X}^F(z)}{zV_i(z)} = \frac{-1}{E(z)} \begin{bmatrix} \bar{K}_1 z + (T\bar{K}_2 - \bar{K}_1) \\ \bar{K}_2(z-1) \end{bmatrix} \qquad (C17)$$

$$E(z) = z^2 - (2-\bar{K}_1-\bar{K}_2 T)z + (1-\bar{K}_1)$$

Similarly substitution of $\bar{K}_2 = 0$ (and $\bar{K}_1 = \bar{K}$) in (C17) and considering only the first component of $\tilde{X}$ result in the transfer function of the first order filter. This after cancellation of the common (z-1) term may be written as,

$$A\ \frac{\tilde{X}^F(z)}{zV_i(z)} = -\frac{\bar{K}}{z-(1-\bar{K})} \qquad (C18)$$

In the same manner the transfer functions $\eta(z)/V_i(z)$ can be obtained from (C7) by substitution of $\bar{K}_3 = 0$ or $\bar{K}_2 = \bar{K}_3 = 0$ respectively for the second order and first order filter respectively. Furthermore, as (C14) is applicable to the smoother of any order, a minor modification of (C15), (C16) also yields the smoother transfer functions for lower order estimators.

Appendix D: Flow Chart of Simulation Program for Smoothers

The flow chart of the computer simulation program SIM developed on the VAX system is given in Figure 25. The program contains both the time domain and frequency domain analysis of the smoothers.

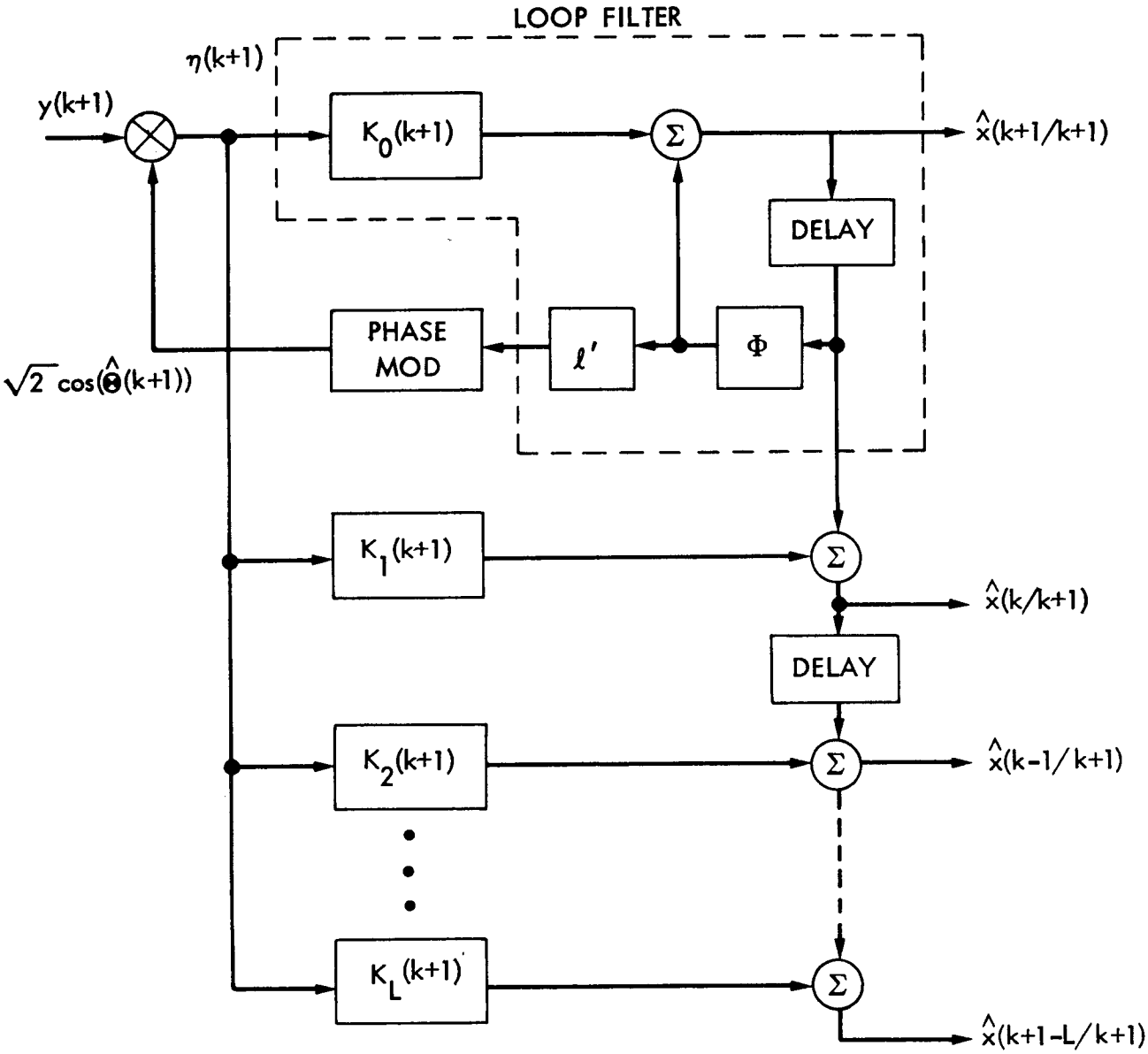

Figure 1. Smoother Implementation

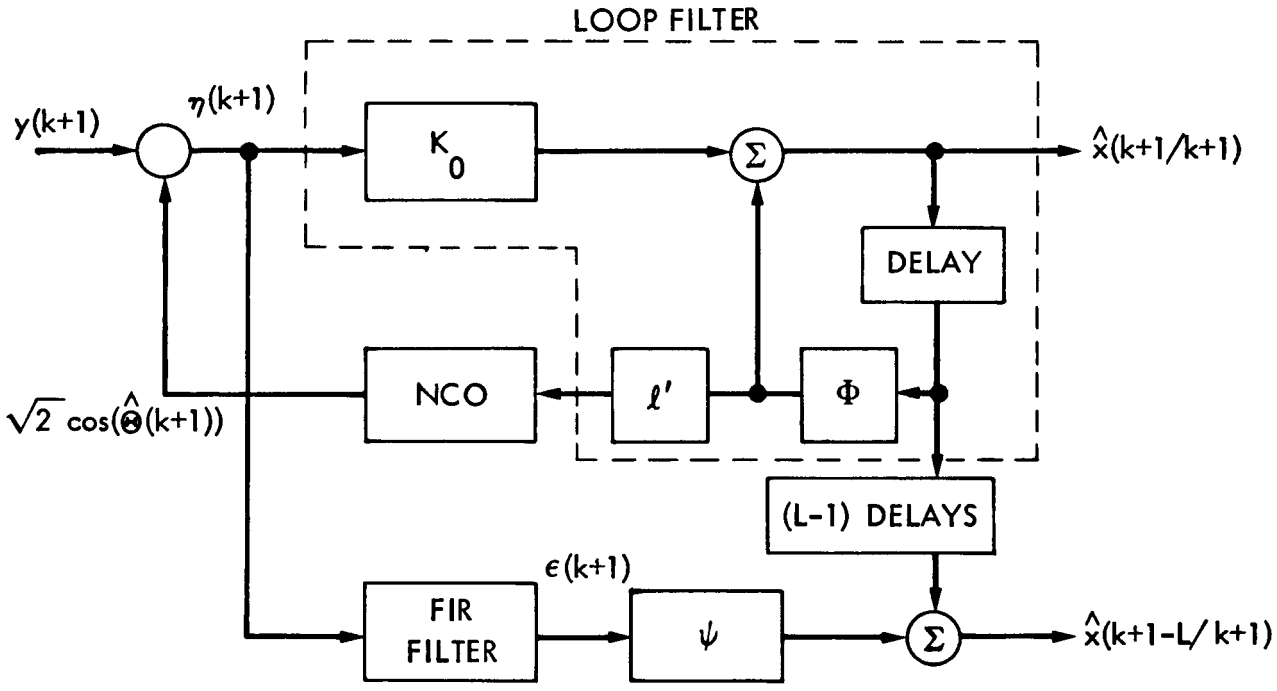

Figure 2. An Equivalent and Simpler Implementation of the Smoother

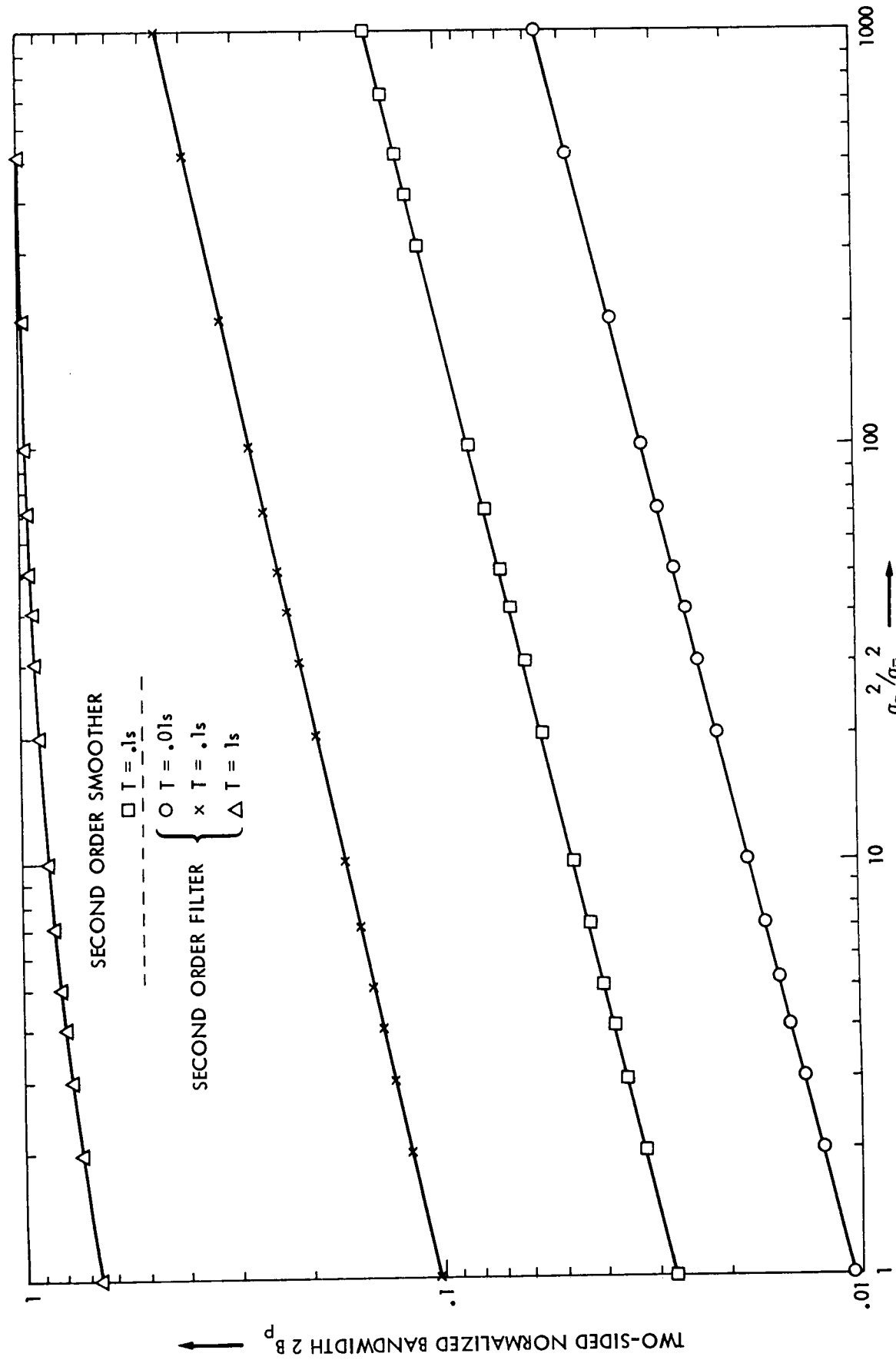

Figure 3. Normalized Loop Noise Bandwidth of the Second Order Filter/Smoother vs $(\sigma_a^2/\sigma_{\dot{v}}^2)$

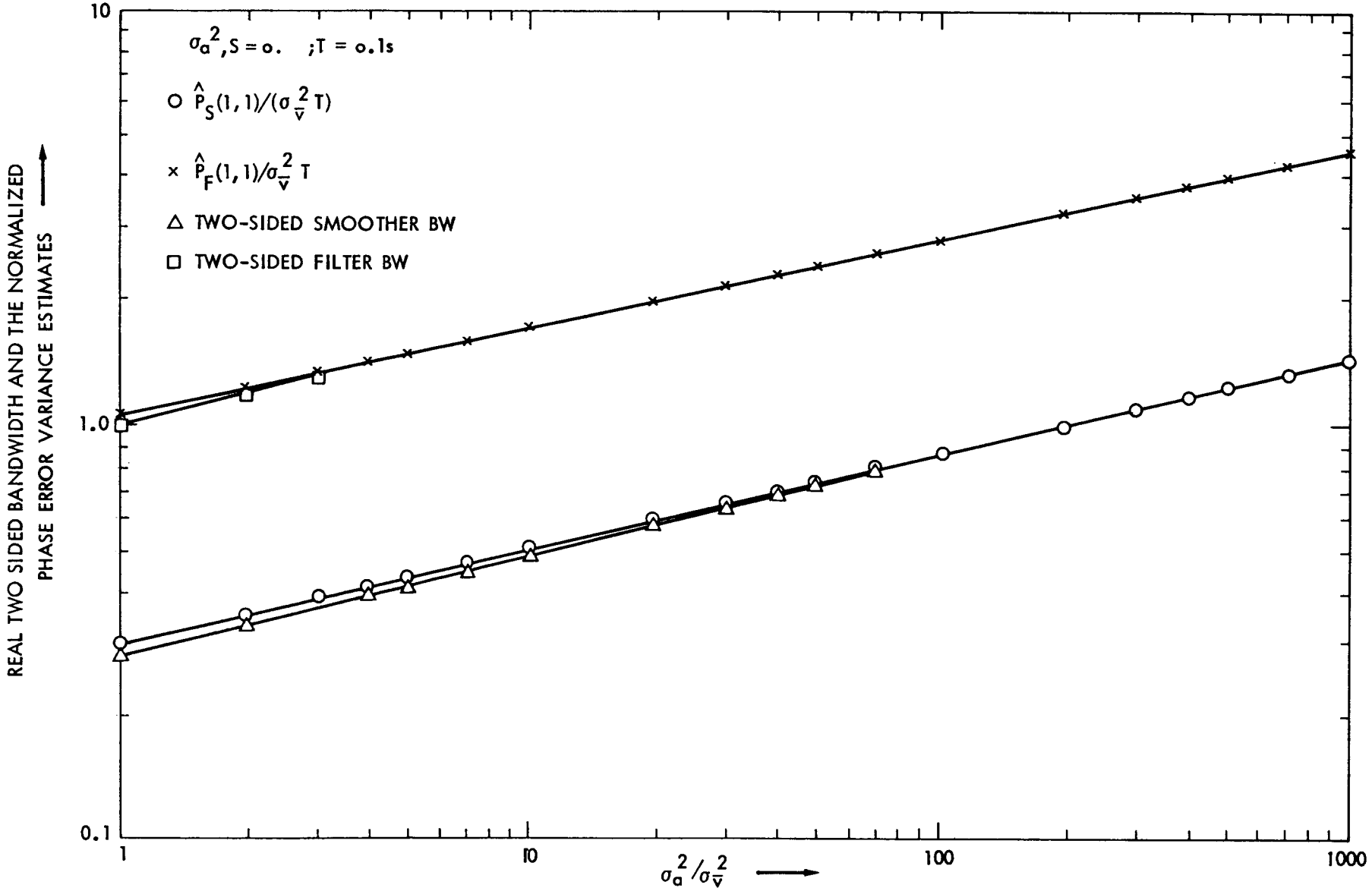

Figure 4. Real Two Sided Bandwidth and the Normalized Phase Error Variance vs $(\sigma_a^2/\sigma_{\bar{v}}^2)$

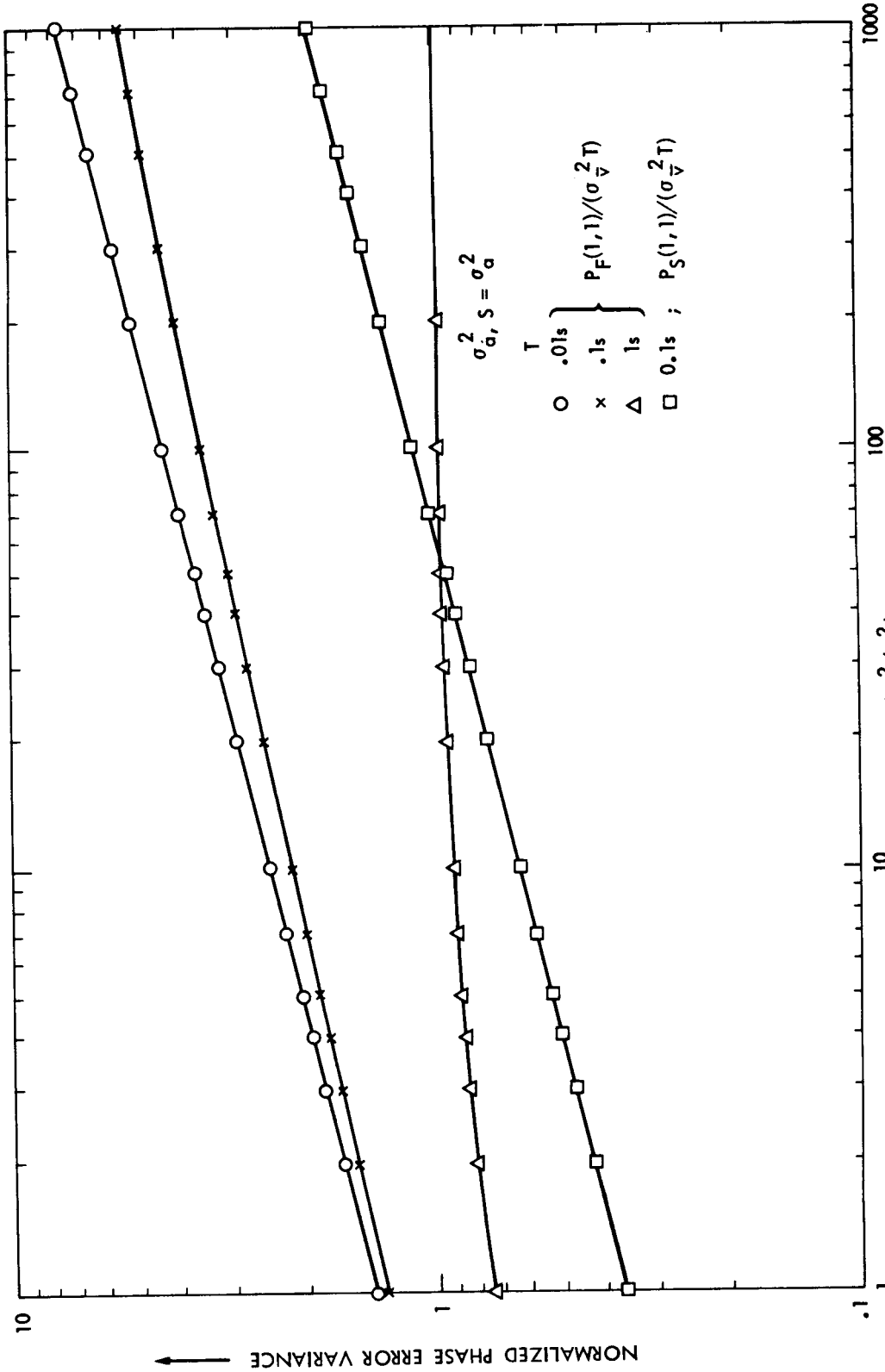

Figure 5. Normalized Phase Error Variance vs $(\sigma_a^2/\sigma_{\bar{v}}^2)$ With $\sigma_{a,S}^2 = \sigma_a^2$

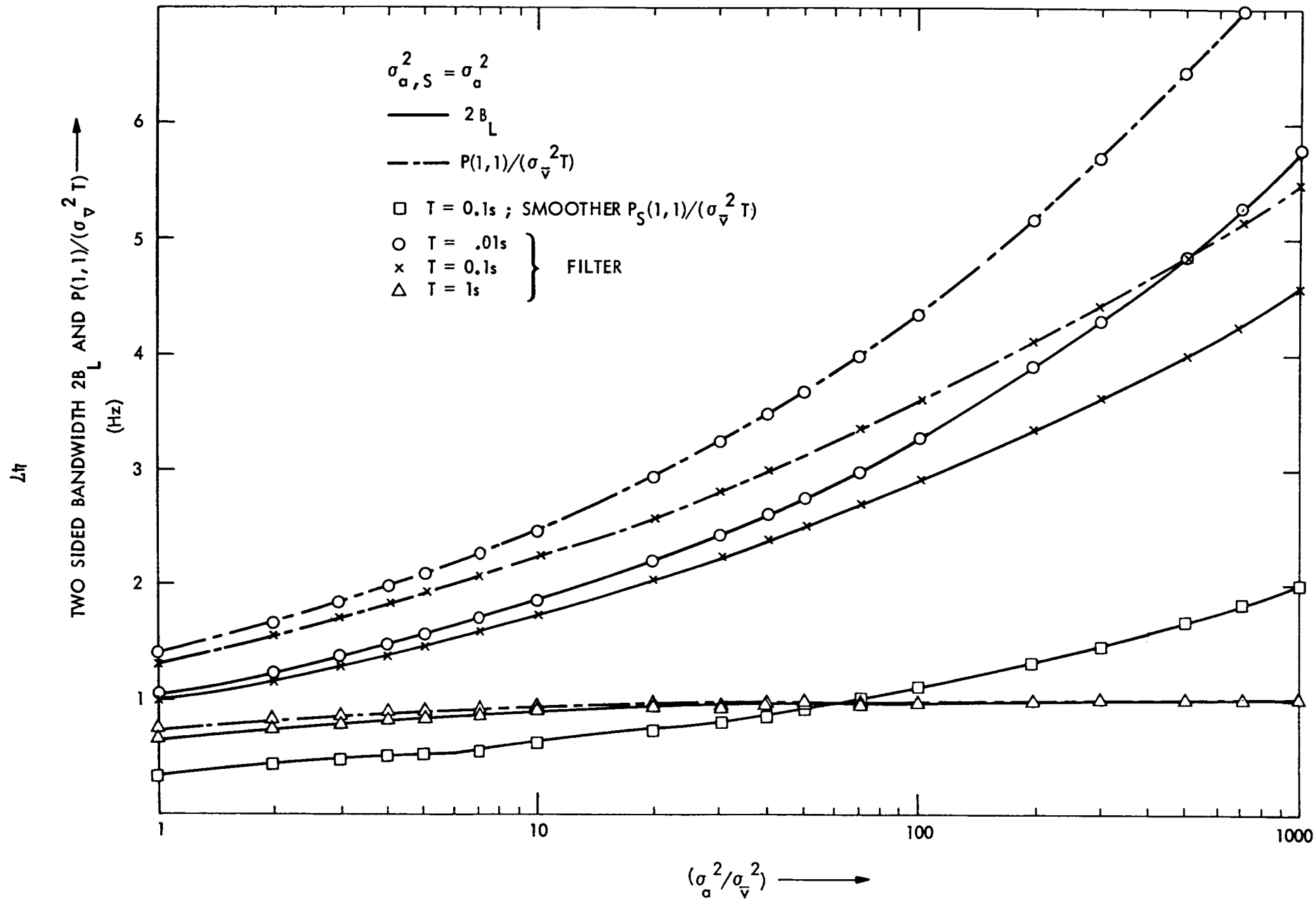

Figure 6. Comparison of Filter Performance With and Without Process Noise

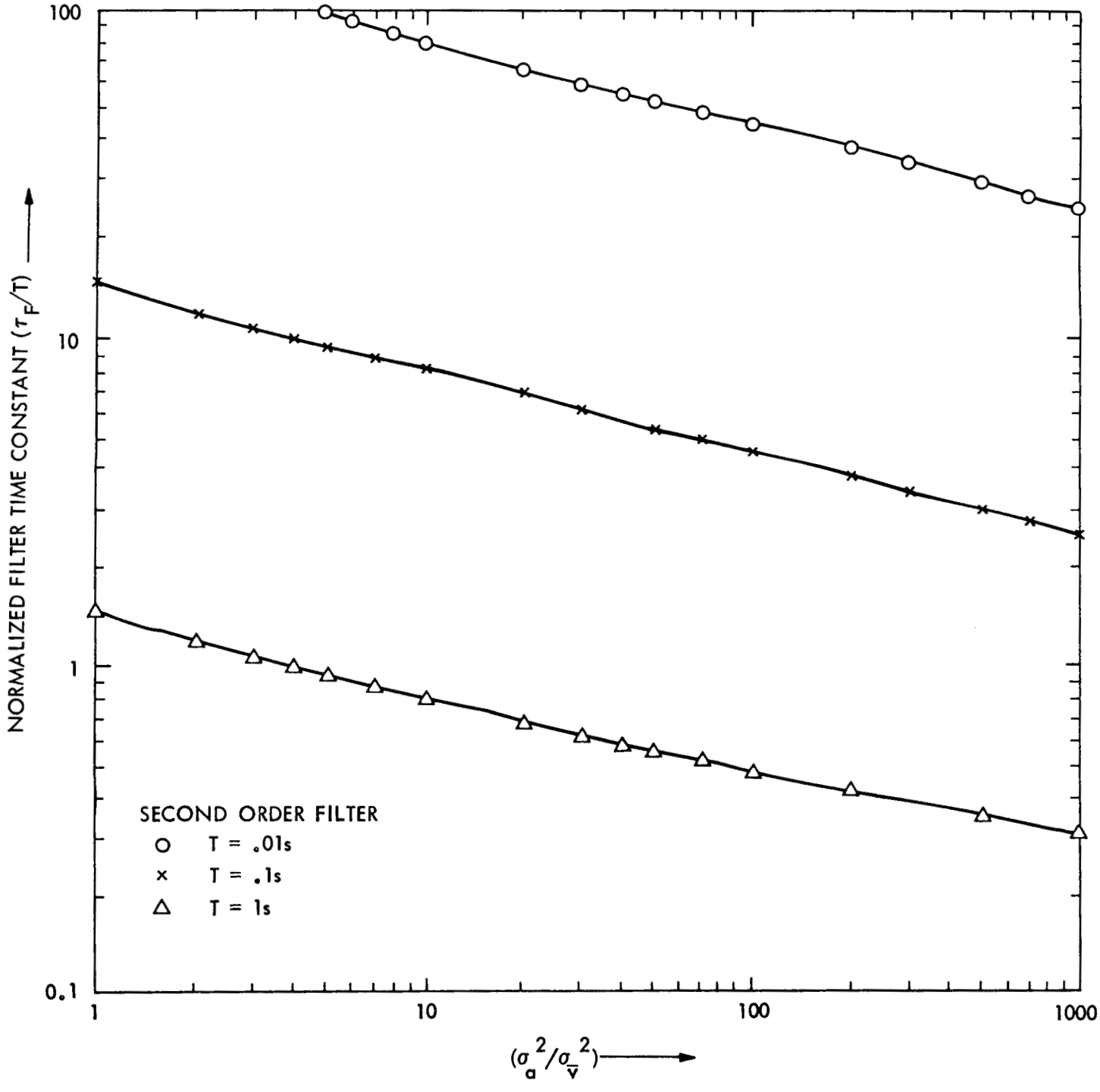

Figure 7. Normalized Filter Time Constant vs $(\sigma_a^2/\sigma_{\bar{v}}^2)$

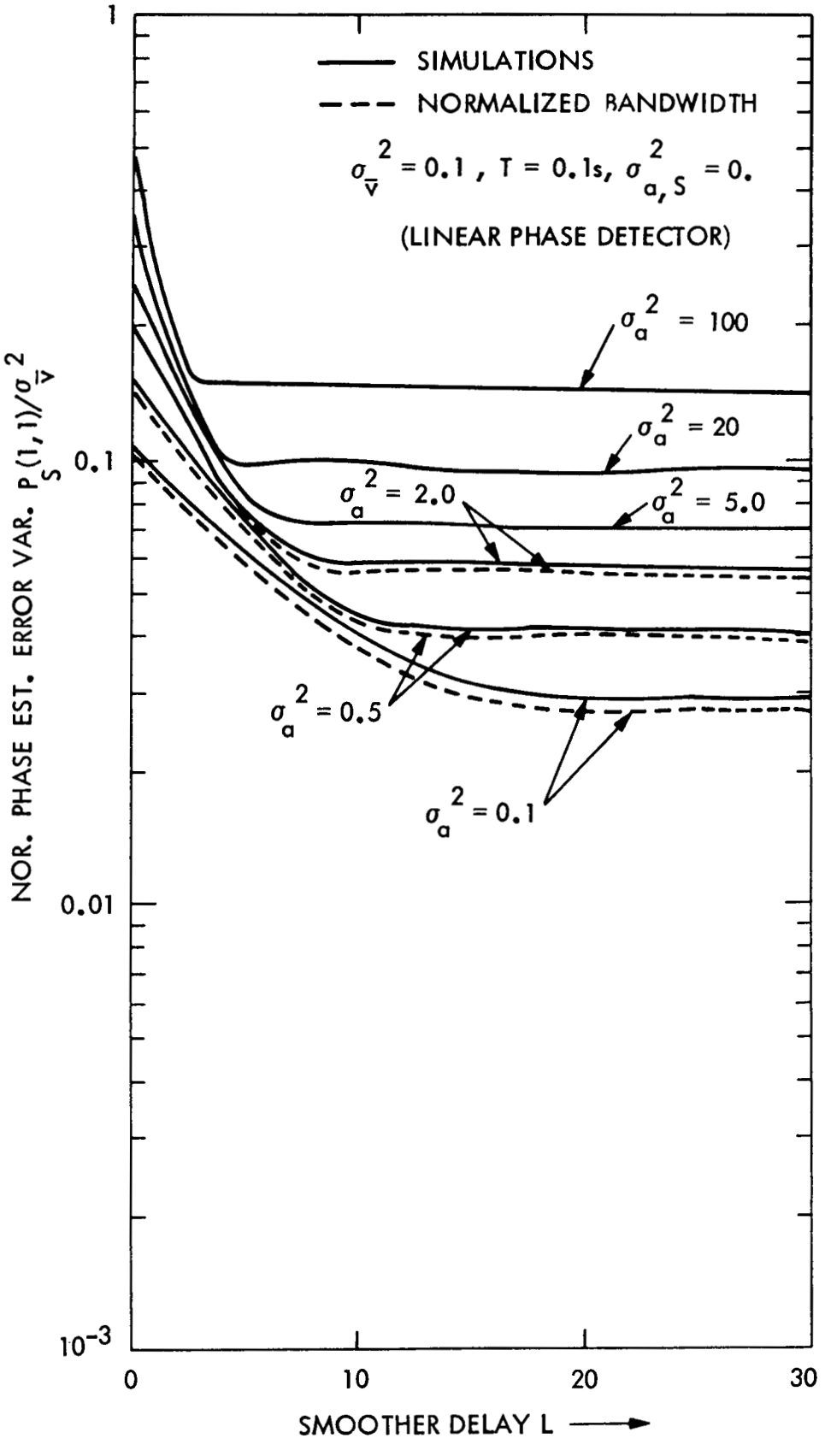

Figure 8. Smoother Estimation Error Variance vs Smoother Delay

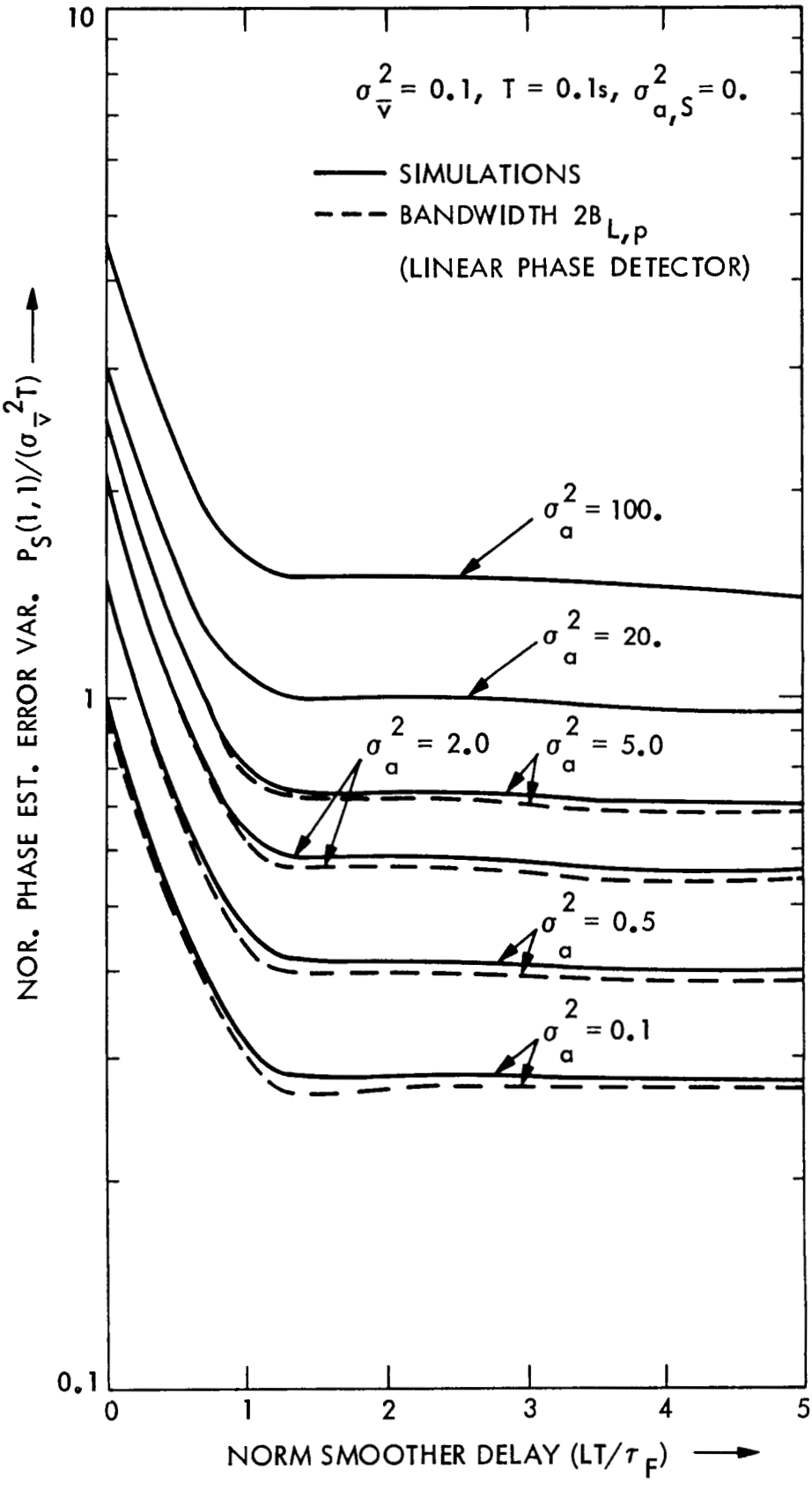

Figure 9. Normalized Smoother Estimation Error Variance vs Normalized Delay

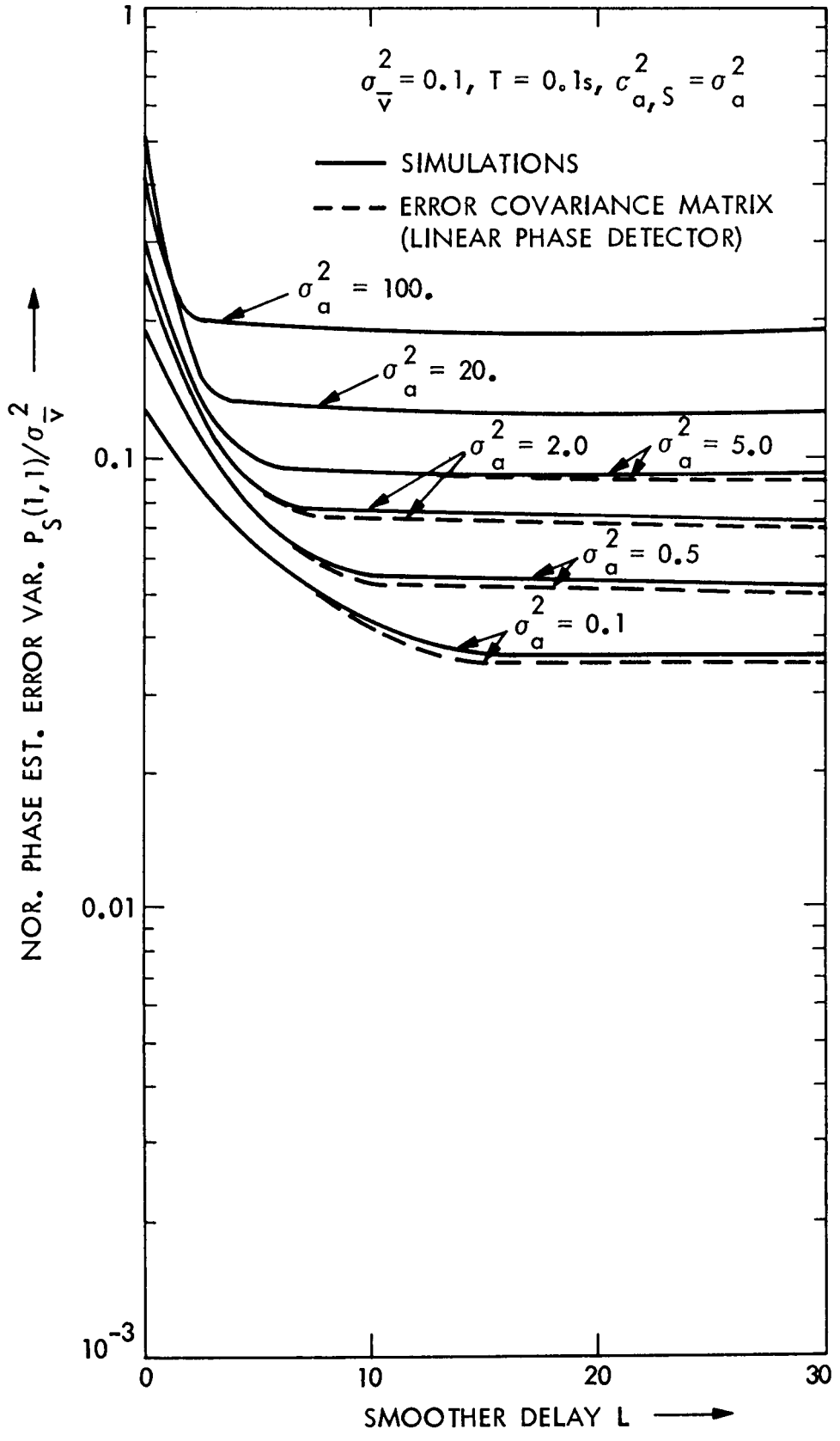

Figure 10. Smoother Estimation Error Variance vs Smoother Delay

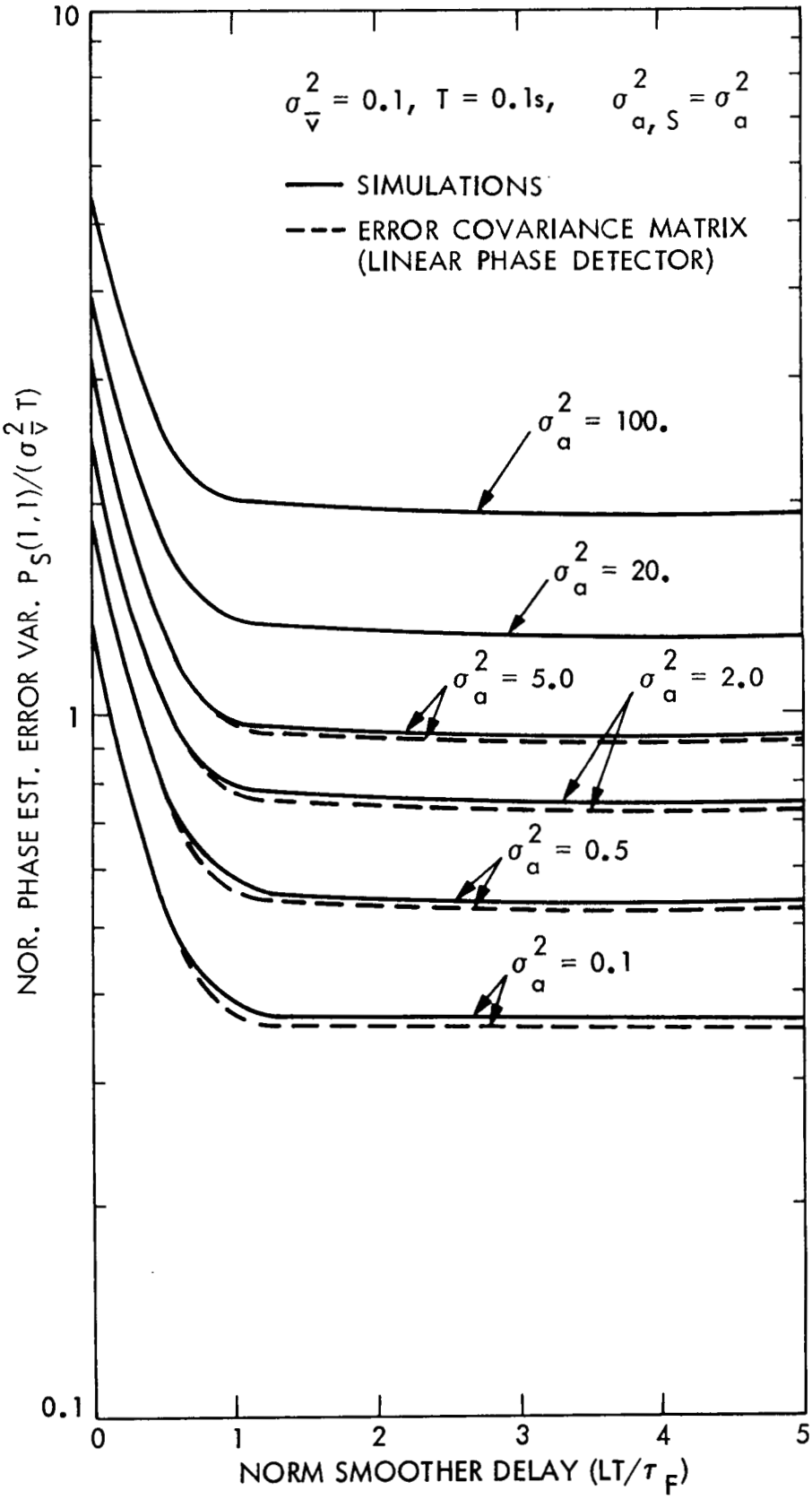

Figure 11. Normalized Smoother Estimation Error Variance vs Normalized Delay

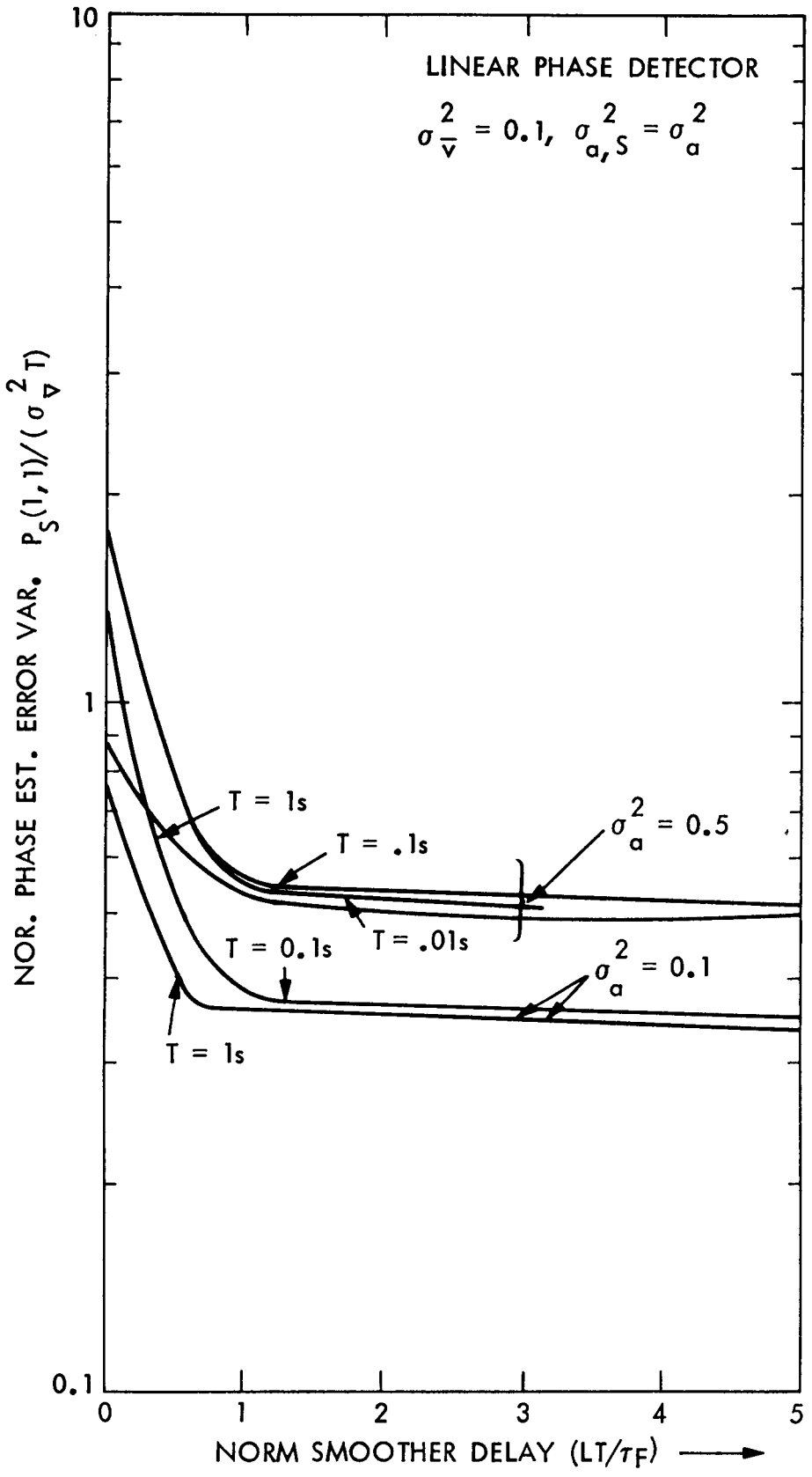

Figure 12. Smoother Performance for Different Sampling Periods

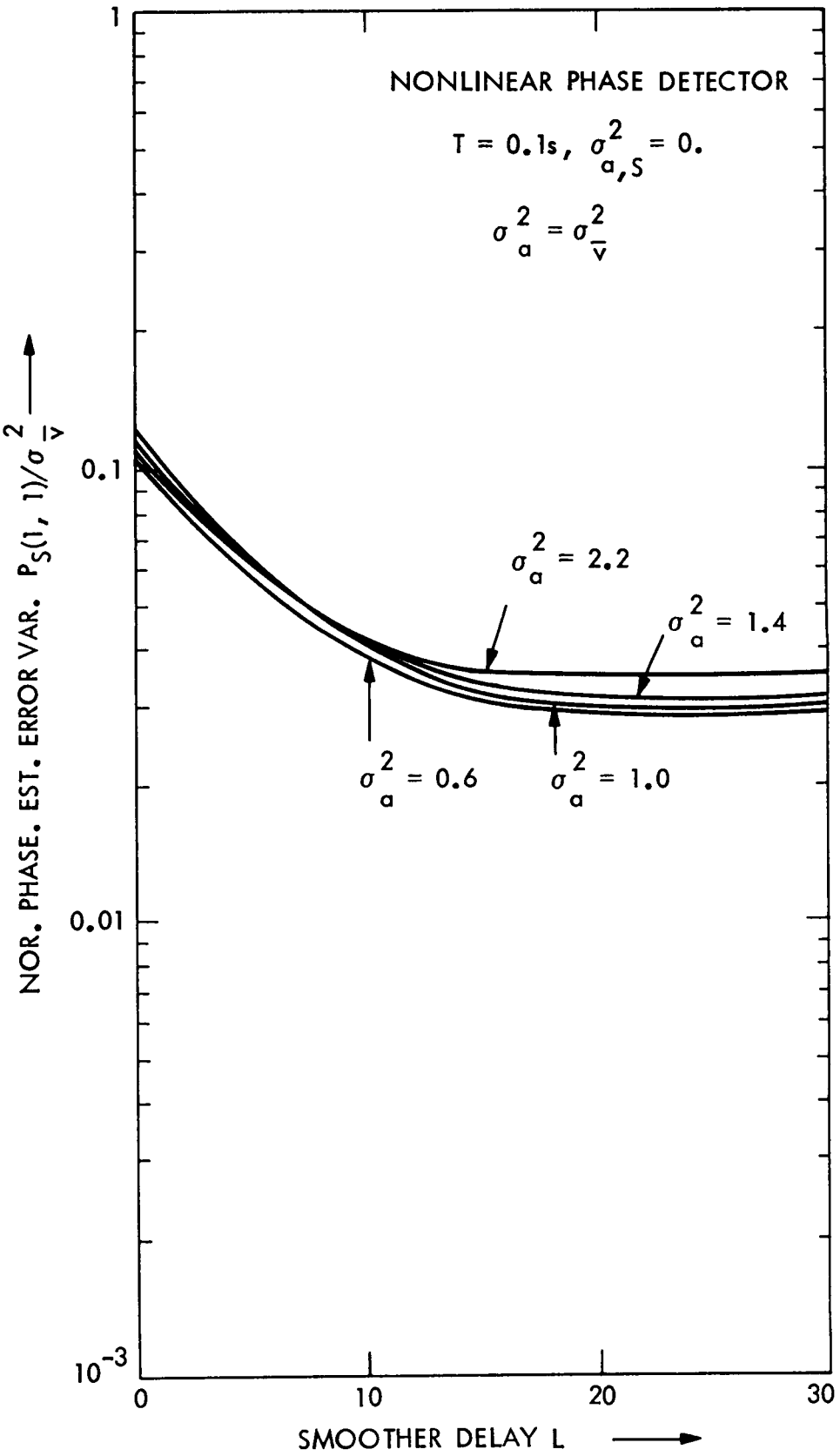

Figure 13. Smoother Phase Estimation Error Variance vs L (Nonlinear Detector With $\sigma^2_{a,S} = 0$)

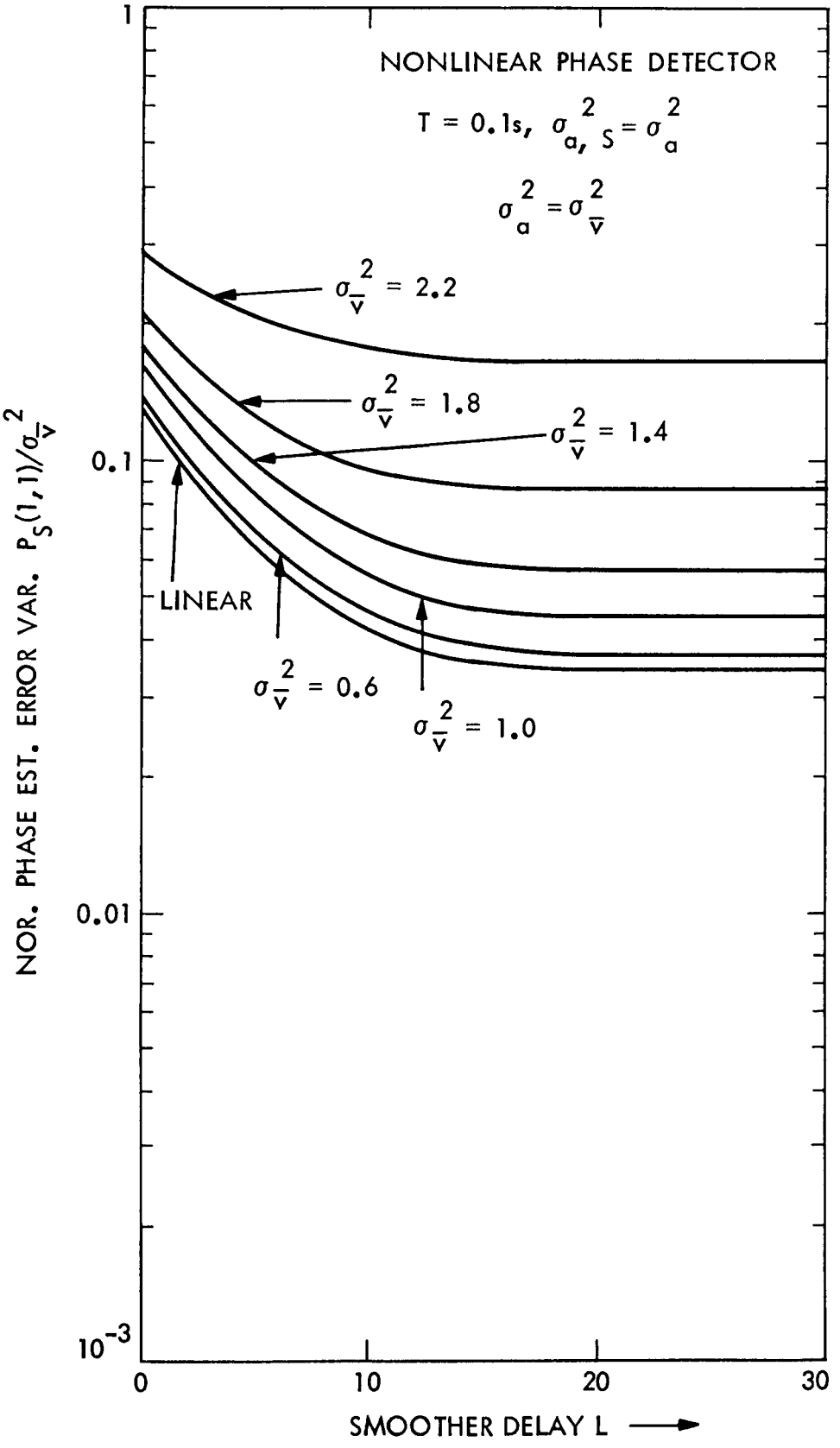

Figure 14. Smoother Phase Estimation Error Variance vs Delay (Nonlinear Detector)

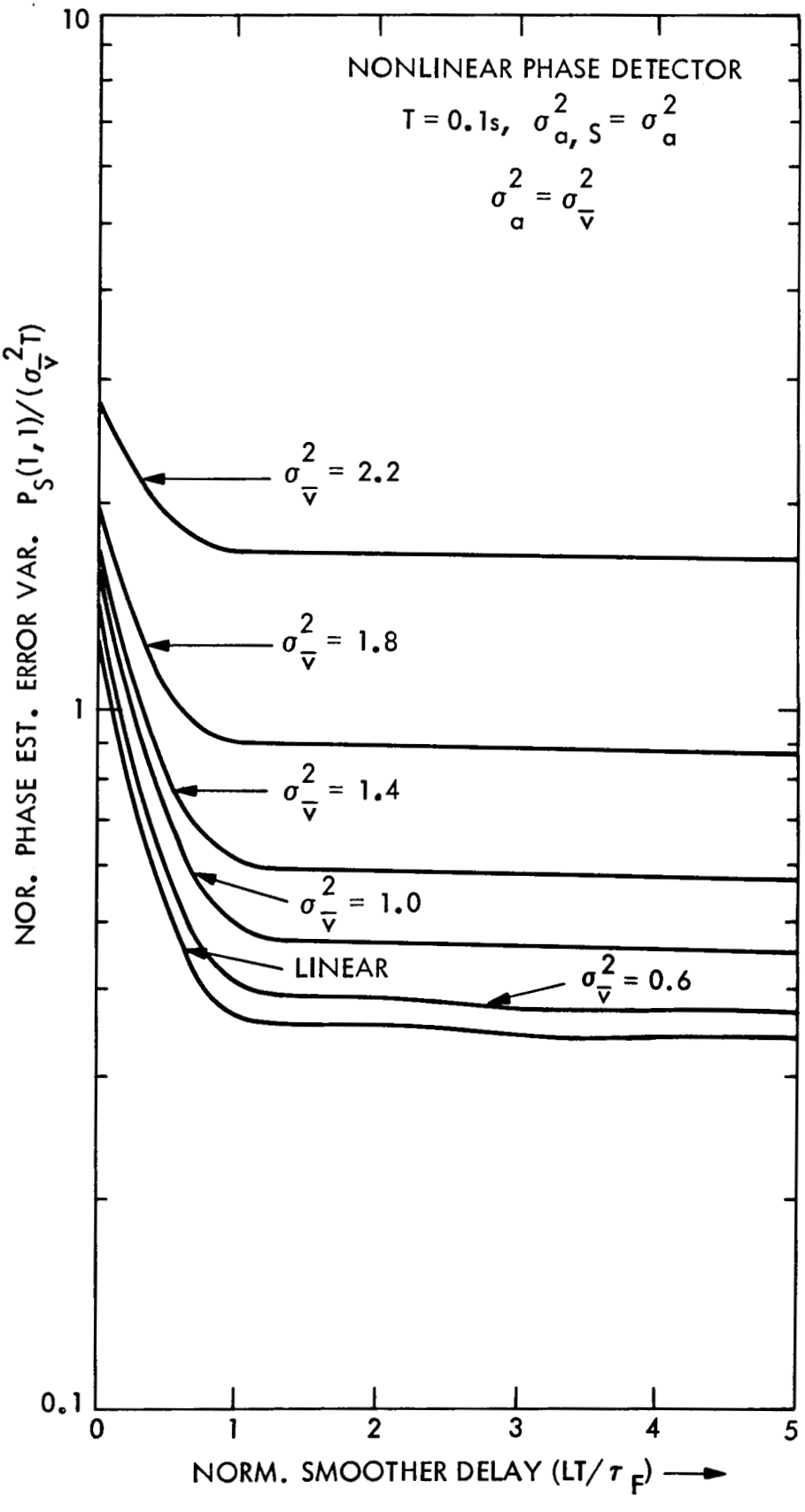

Figure 15. Normalized Phase Estimation Error vs Normalized Delay (Nonlinear Phase Detector)

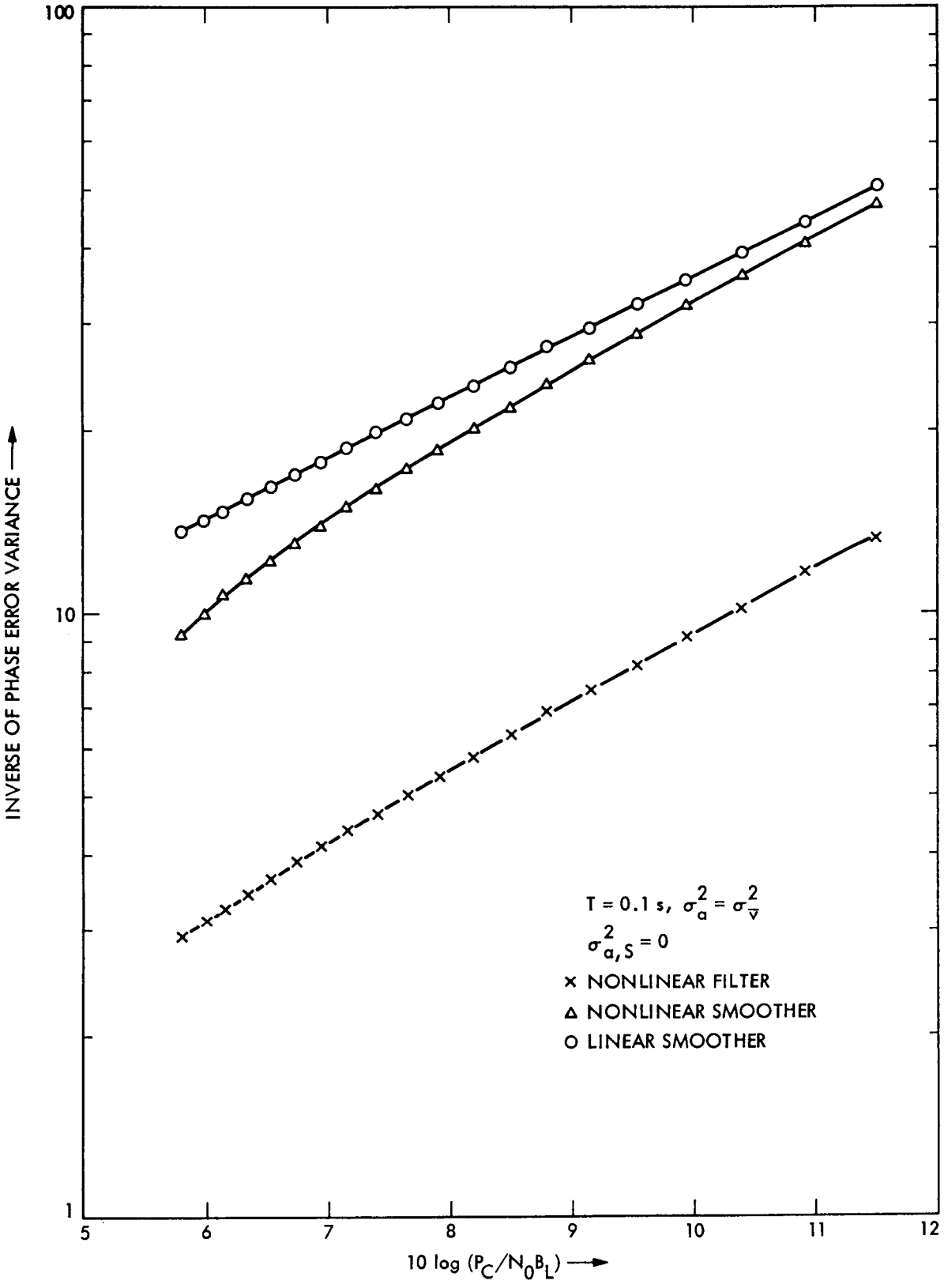

Figure 16. Comparison of Smoother Performance With Linear and Nonlinear Phase Detectors ($\sigma_{a,S}^2 = 0$)

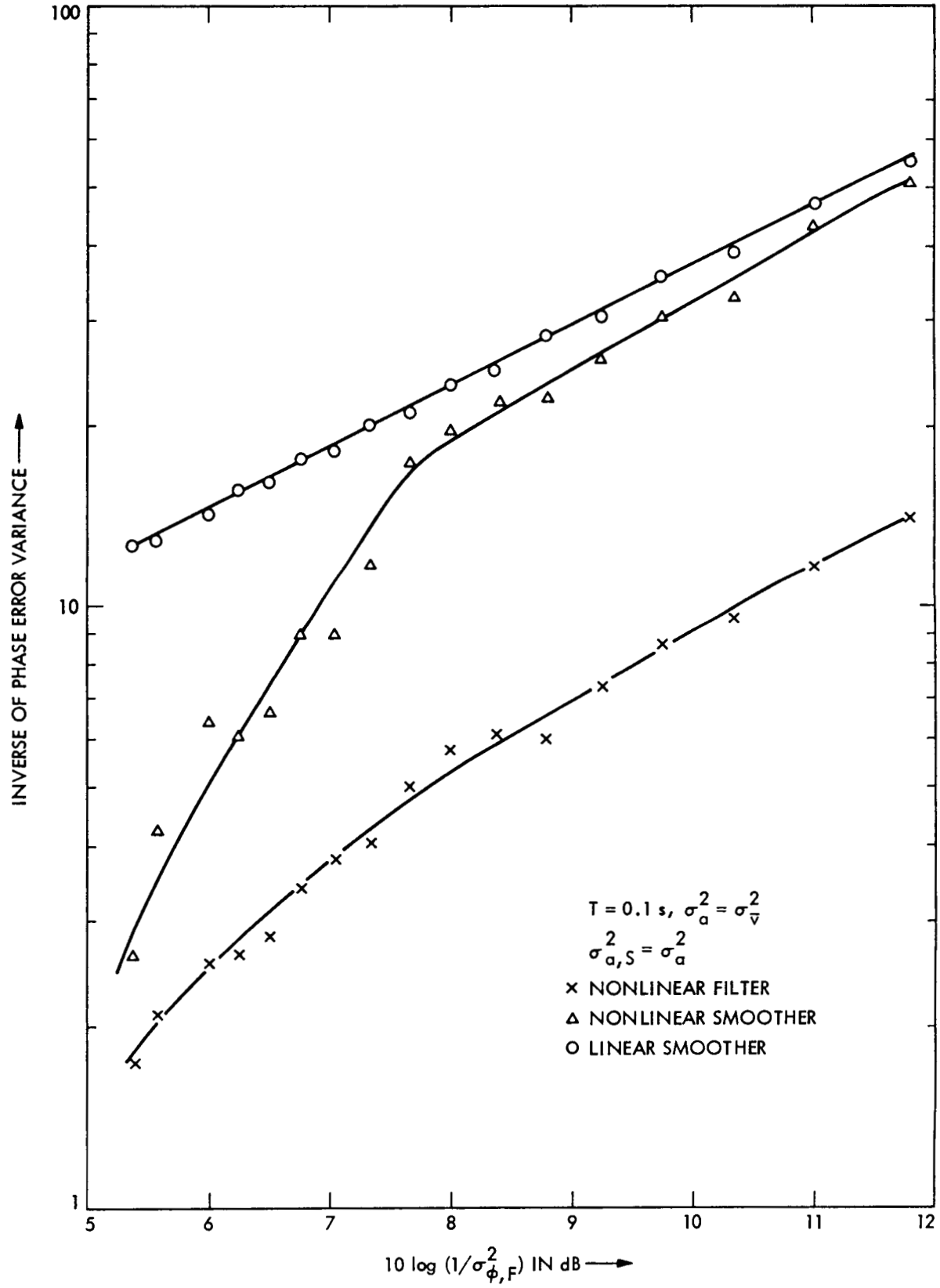

Figure 17. Comparison of Smoother Performance With Linear and Nonlinear Phase Detectors ($\sigma^2_{a,S} \neq 0$)

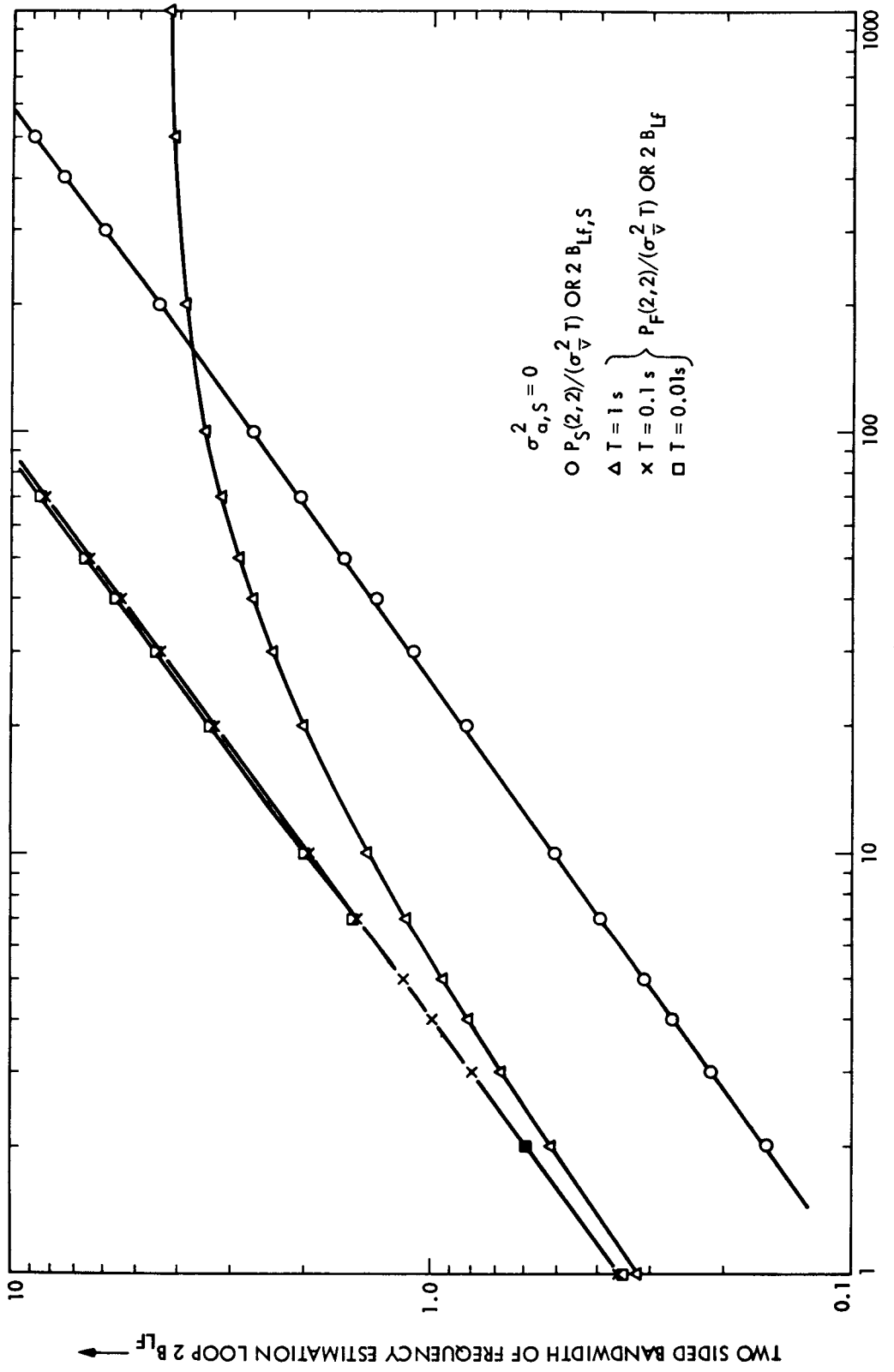

Figure 18. Frequency Estimation Loop Bandwidth vs $(\sigma_a^2/\sigma_{\dot{v}}^2)$

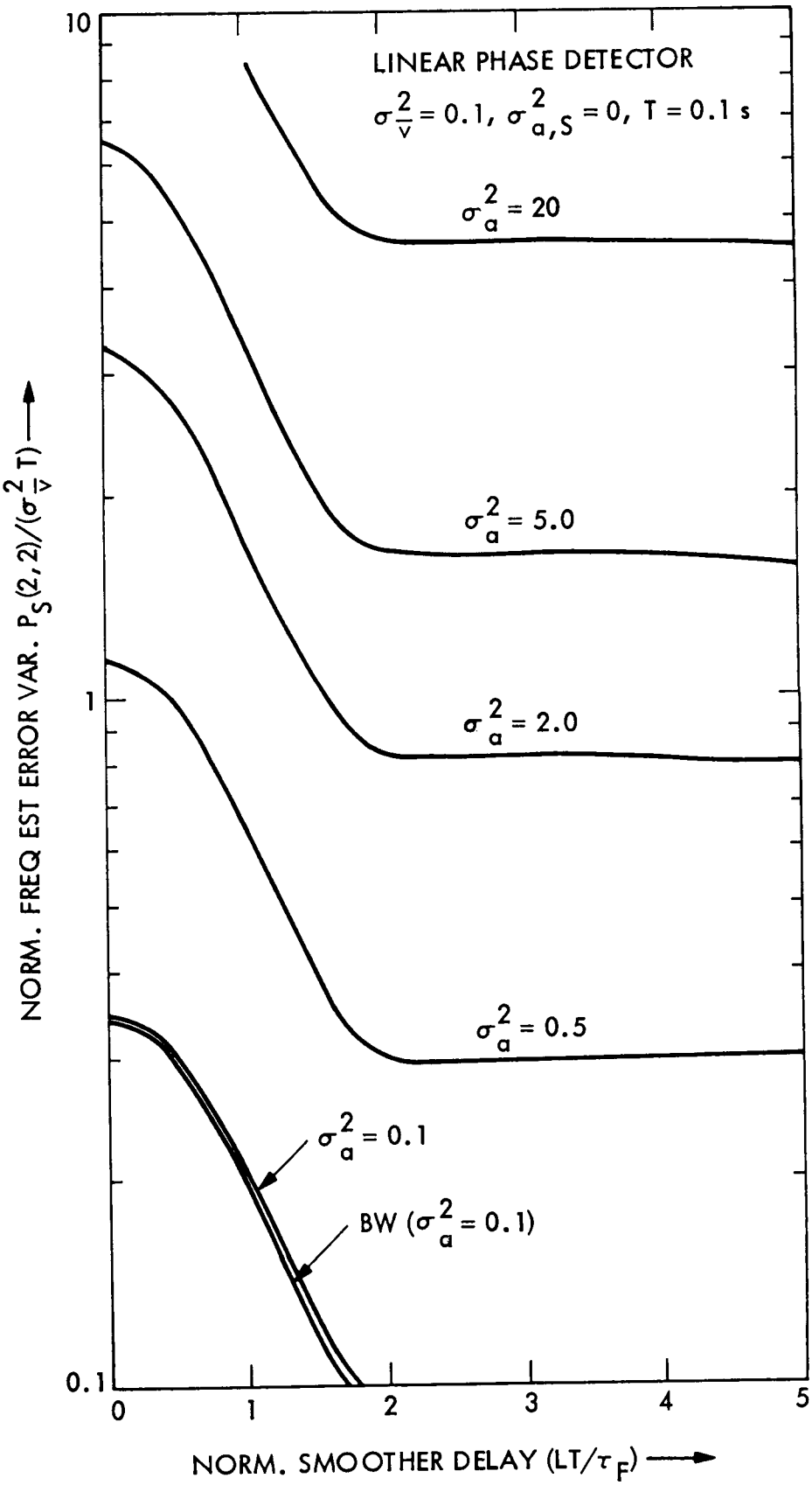

Figure 19. Normalized Frequency Estimation Error Variance vs Normalized Delay ($\sigma_{a,S}^2 = 0$)

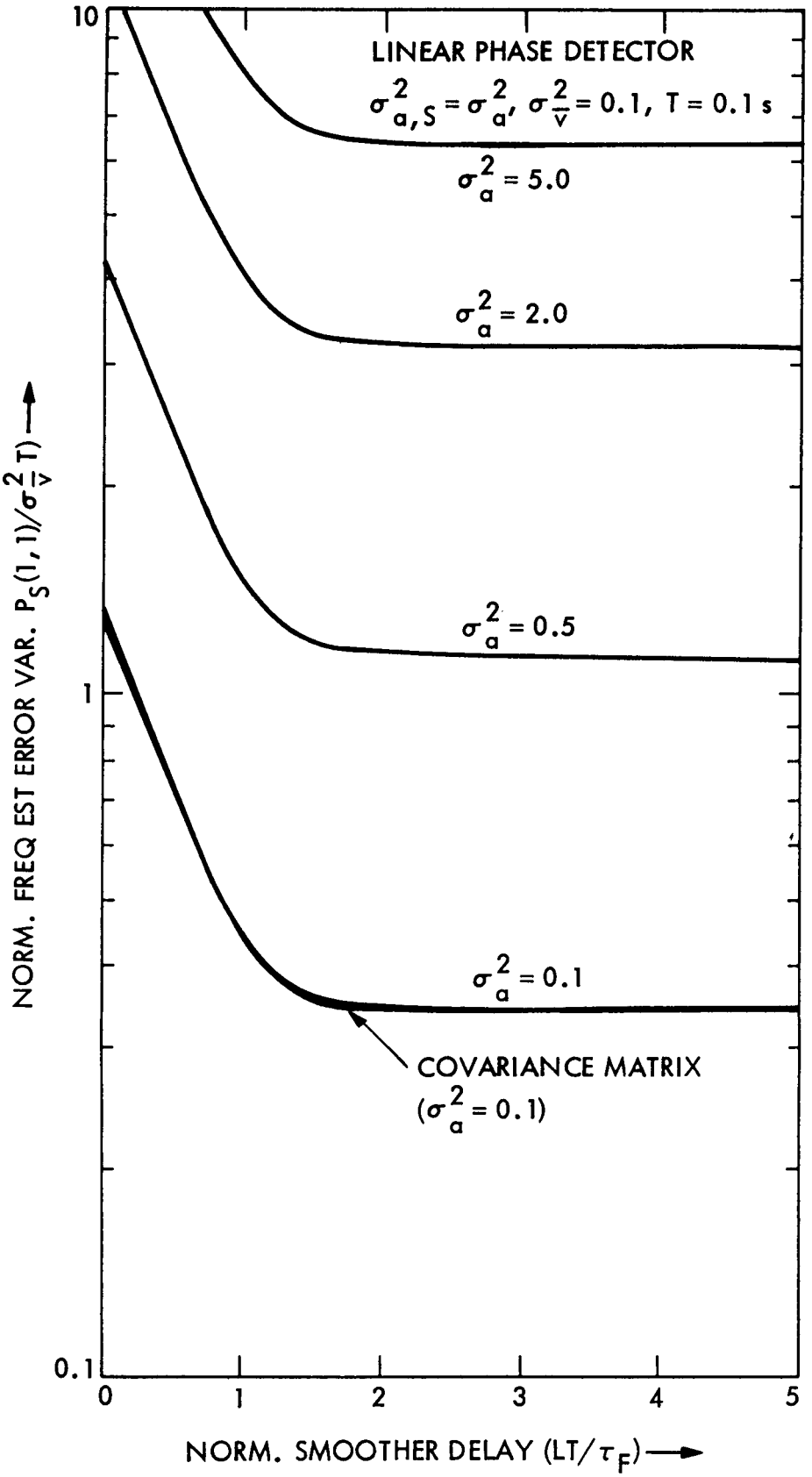

Figure 20. Normalized Frequency Estimation Error vs Normalized Delay ($\sigma^2_{a,S} = \sigma^2_a$)

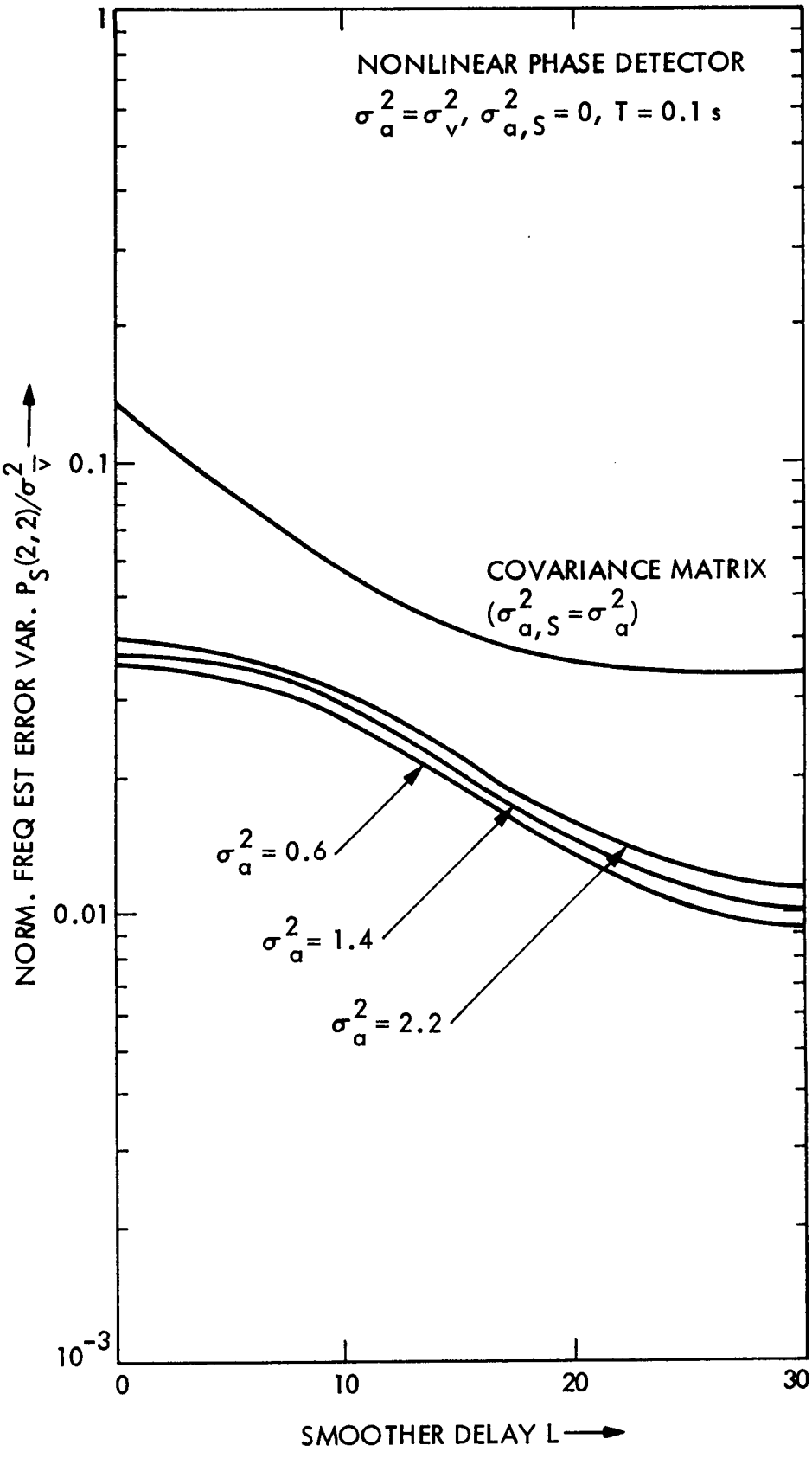

Figure 21. Normalized Frequency Estimation Error Variance With Nonlinear Phase Detector ($\sigma_{a,S}^2 = 0$)

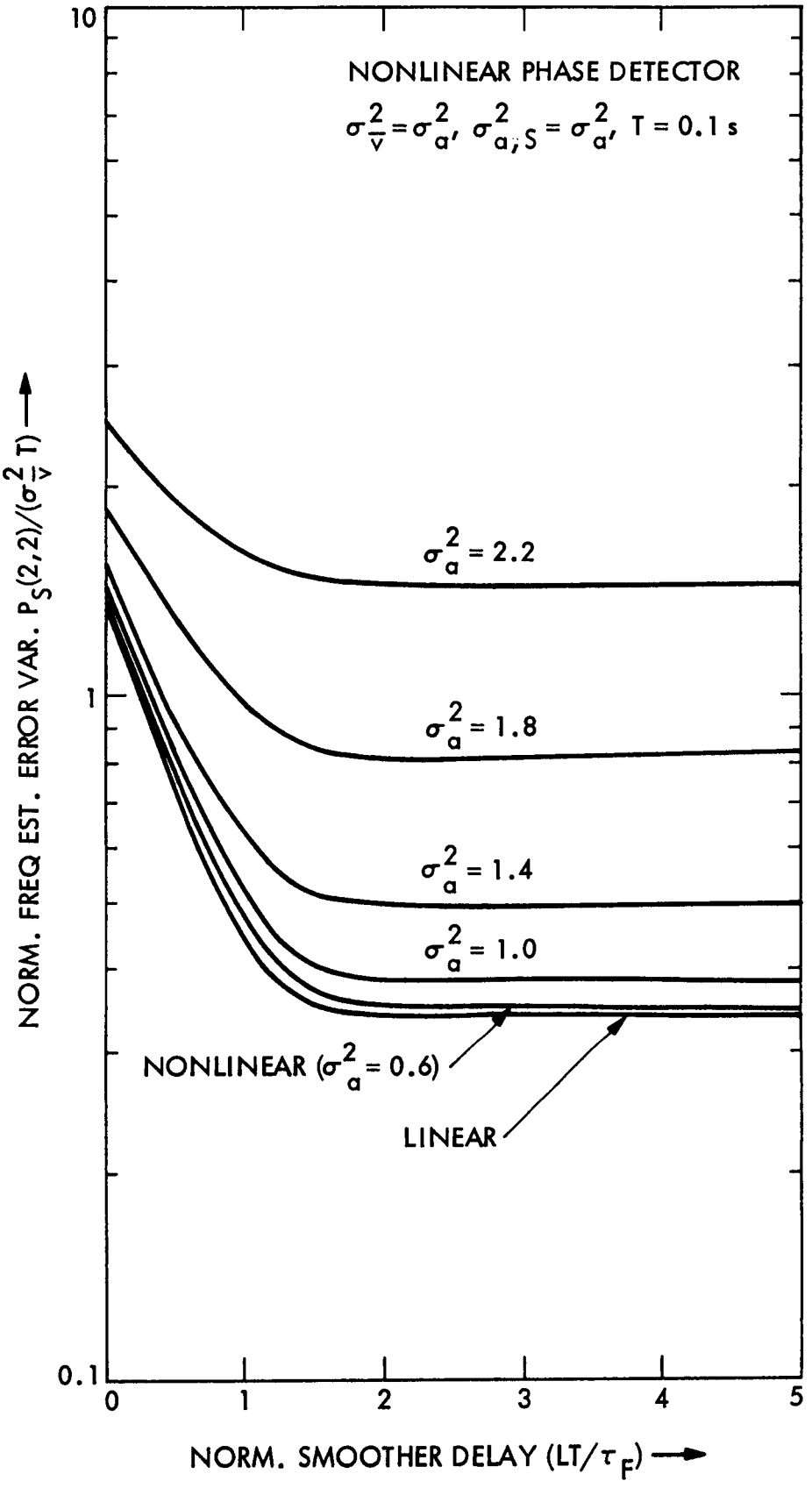

Figure 22. Normalized Frequency Estimation Error Variance With Nonlinear Phase Detector ($\sigma_{a,S}^2 = \sigma_a^2$)

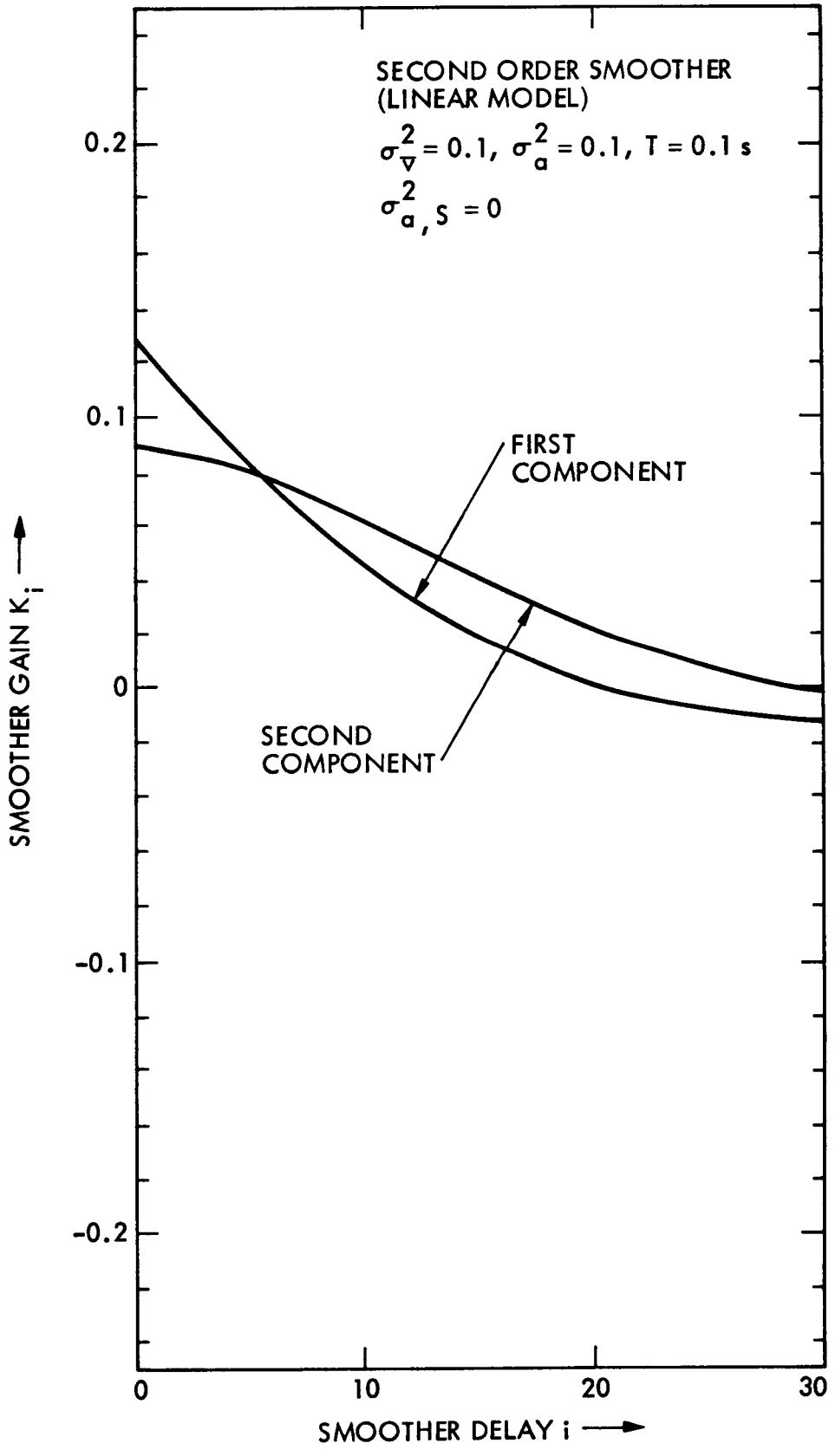

Figure 23. Smoother Gain K_i; $1 \leq i \leq L$ ($\sigma_a^2/\sigma_v^2 = 1$)

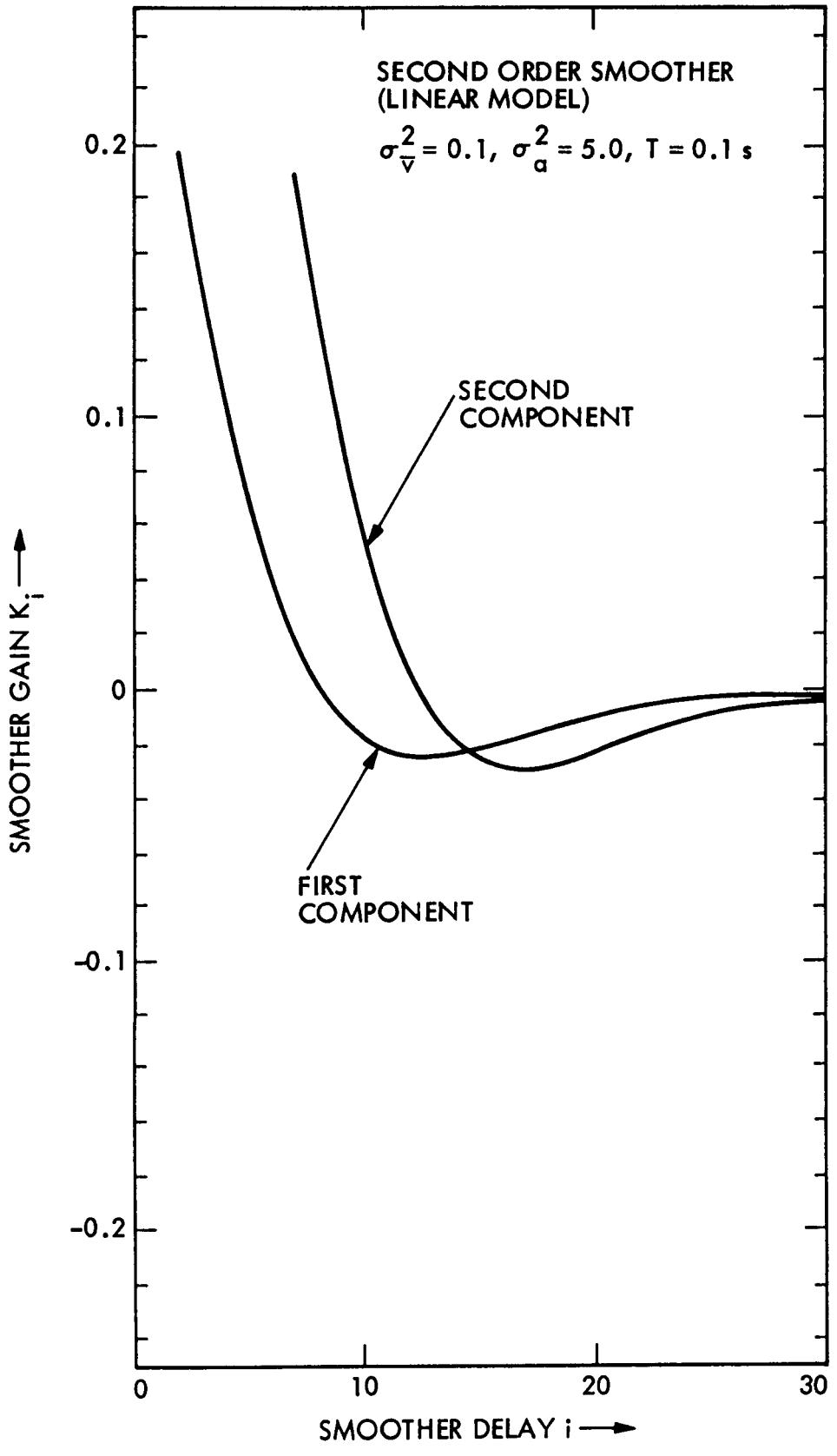

Figure 24. Smoother Gain K_i; $1 \leq i \leq L$ ($\sigma_a^2/\sigma_v^2 = 50$)

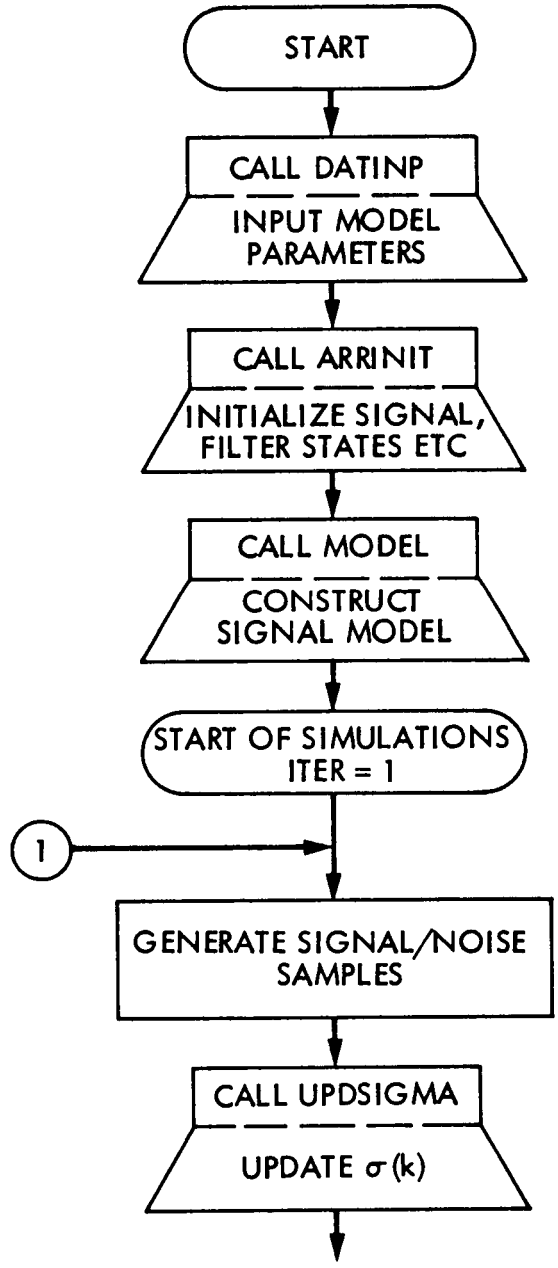

Figure 25. Flow Chart of Simulation Program for Smoothers

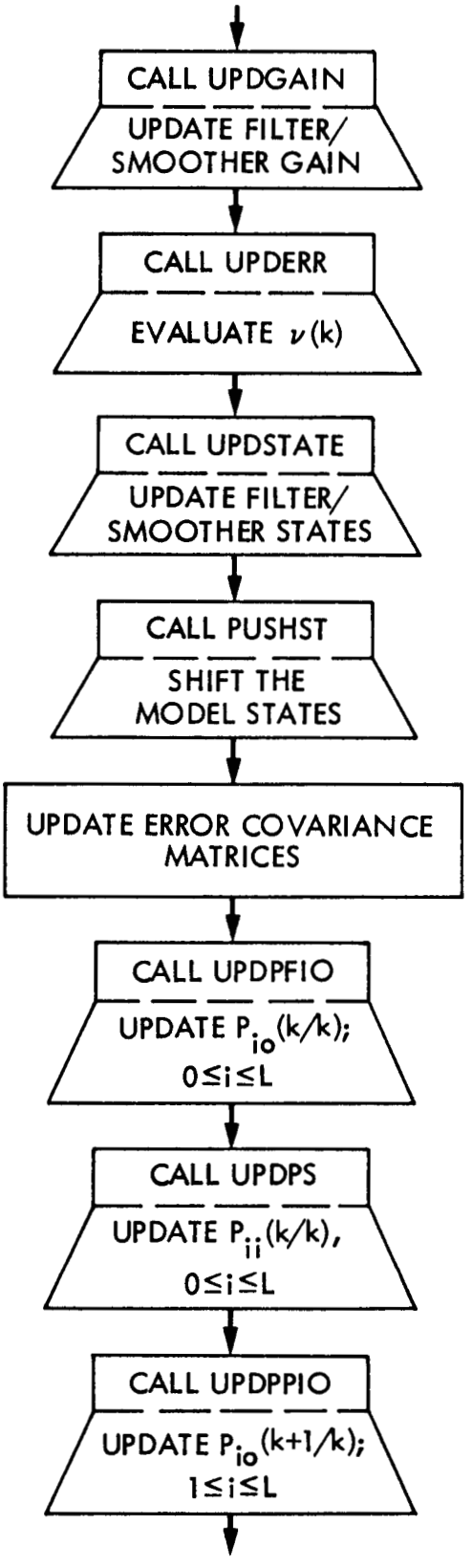

Figure 25. Flow Chart of Simulation Program for Smoothers (Contd)

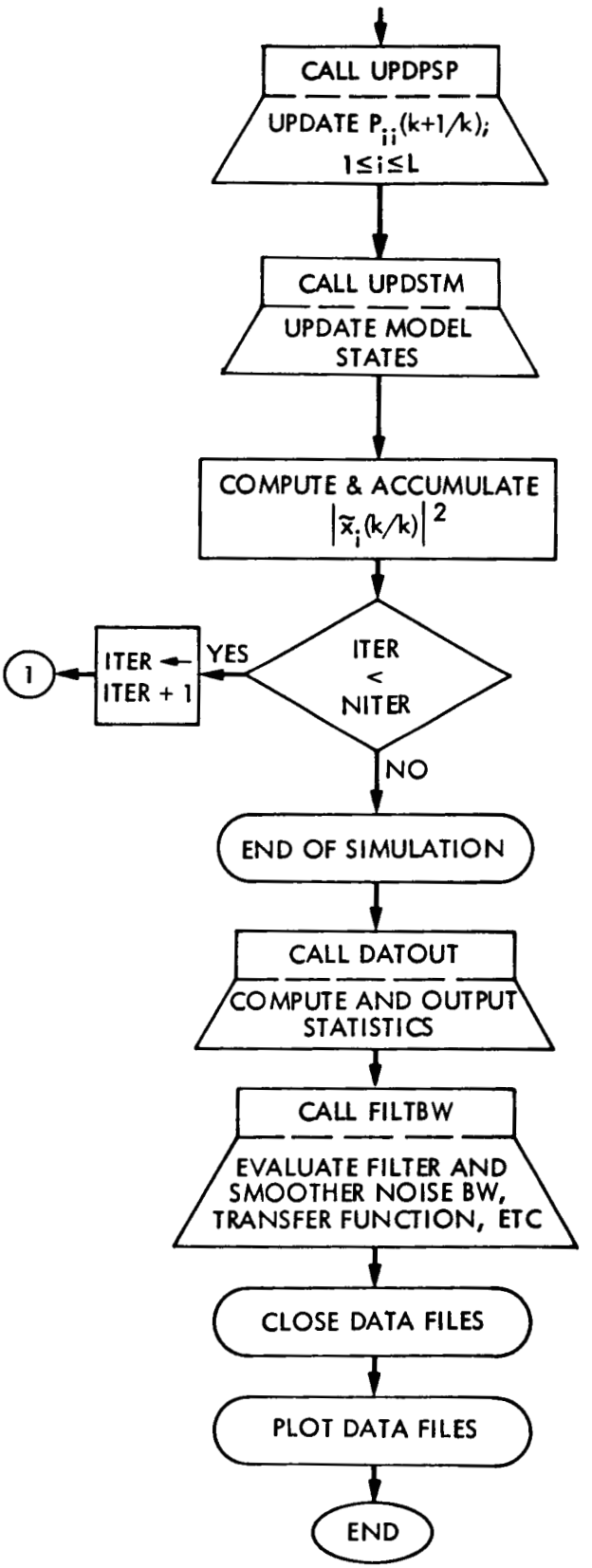

Figure 25. Flow Chart of Simulation Program for Smoothers (Contd)

TECHNICAL REPORT STANDARD TITLE PAGE

1. Report No. JPL Publication 87-10	2. Government Accession No.	3. Recipient's Catalog No.
4. Title and Subtitle Optimum Filters and Smoothers Design for Carrier Phase and Frequency Tracking		5. Report Date May 1, 1987 6. Performing Organization Code
7. Author(s) Rajendra Kumar		8. Performing Organization Report No.
9. Performing Organization Name and Address JET PROPULSION LABORATORY California Institute of Technology 4800 Oak Grove Drive Pasadena, California 91109		10. Work Unit No. 11. Contract or Grant No. NAS7-918 13. Type of Report and Period Covered JPL Publication
12. Sponsoring Agency Name and Address NATIONAL AERONAUTICS AND SPACE ADMINISTRATION Washington, D.C. 20546		14. Sponsoring Agency Code RE210 BG-310-30-70-84-02

15. Supplementary Notes

16. Abstract

The report presents the application of fixed lag smoothing algorithms to the problem of estimation of the phase and frequency of a sinusoidal carrier received in the presence of process noise and additive observation noise. A suboptimal structure consists of a phase-locked loop (PLL) followed by a post-loop correction to the phase and frequency estimates. When the PLL is operating under high signal-to-noise ratio, the phase detector is approximately linear, and the smoother equations then correspond to the optimal linear equations for an equivalent linear signal model. The performance of such a smoother can be predicted by linear filtering theory. However, if the PLL is operating near the threshold region of the signal-to-noise ratio, the phase detector cannot be assumed to be linear. Then the actual performance of the smoother can significantly differ from that predicted by linear theory. In this report we present both the theoretical and simulated performance of such smoothers derived on the basis of various maodels for the phase and frequency processes.

17. Key Words (Selected by Author(s))	18. Distribution Statement
Communications Computer Programming and Software	Unclassified - Unlimited

19. Security Classif. (of this report)	20. Security Classif. (of this page)	21. No. of Pages	22. Price
Unclassified	Unclassified	73	